1 **Title:** *Corylus avellana* disease management: using metagenomics to illuminate the rhizosphere
2 microbiome of *Corylus*
3
4 **Authors:** John K. Robinson[1], John Steele[1], Thomas J. Molnar[2], Sharon Regan[1], George C.
5 diCenzo[1*]
6
7 **Affiliations:** [1] Department of Biology, Queen's University, Kingston, Ontario, Canada
8 [2] Department of Plant Biology, Rutgers University, Newark, New Jersey, USA
9
10 *** Corresponding author:** George C. diCenzo, george.dicenzo@queensu.ca
11
12 **Keywords:** Hazelnut, Rhizosphere, Metagenomics, Microbiome, Plant-Microbe Interaction

ABSTRACT

The European hazelnut, *Corylus avellana*, is one of the most economically important tree nut crops globally. The biotrophic ascomycete pathogen *Anisogramma anomala*, found naturally associated with wild *C. americana*, continues to pose a significant threat to European hazelnut production across North America. Rhizosphere microorganisms have demonstrated the capacity to impact diverse plant features and serve as an important resource for the improvement of plant disease outcomes. Here, metagenomics was used to examine the taxonomic and functional features of the rhizosphere microbial communities of hazelnut trees differing in their levels of resistance to *A. anomala*: highly tolerant *Corylus americana*, and resistant and susceptible *Corylus avellana*. No statistically significant differences in microbial alpha diversity or beta diversity were noted between the three rhizosphere groups. Compared to bulk soil, all three rhizosphere groups were enriched for the fungal phylum Basidiomycota and bacterial phylum "*Candidatus* Rokubacteriota". At the genus level, the bacterial genera *Actinospica*, *Occallatibacter*, and "*Candidatus* Sulfotelmatobacter" were under-represented, while the genus *Rhizobacter* was over-represented, in the resistant and susceptible *C. avellana* rhizosphere samples compared to the bulk soil. A total of 45 dereplicated, high-quality metagenome-assembled genomes were generated, corresponding to 41 bacteria and 4 archaea. Many of the metagenome-assembled genomes carried multiple biosynthetic gene clusters, including MAGs corresponding to the genera *Lysobacter* and *Actinospica*. Overall, the low differentiation of the rhizosphere microbiomes of the three hazelnut rhizosphere groups suggest that differences in *A. anomala* disease expression are likely not associated with differences in the rhizosphere microbiome. Nevertheless, the results shed new light on the rhizosphere communities of two species of hazelnut, and woody perennials more broadly, and identify potential avenues for future research into the development of microbial inoculants for *Corylus* spp..

37 **INTRODUCTION**

38 Hazelnut cultivation has a rich history and is still of economic importance in contemporary
39 societies. The European hazelnut *Corylus avellana* has been cultivated since Roman times
40 (Boccacci and Botta 2009) and remains one of the world's principal tree nut crops (Helmstetter et
41 al. 2020). Approximately 70% percent of the world's hazelnuts are presently grown in Turkey
42 (Food and Agricultural Organization of the United Nations 2021), but the future of Turkey's
43 hazelnut industry remains uncertain. To stabilize existing hazelnut production and supply growing
44 global demand, the world's hazelnut orchards must expand across suitable growing regions.
45 Historically, commercial production of *C. avellana* in North America outside of the Pacific
46 Northwest was limited due to the devastating impact of the biotrophic ascomycete pathogen
47 *Anisogramma anomala* (Molnar 2011; Revord et al. 2020; Thompson et al. 1996). Unlike the
48 native but not-commercially amenable American hazelnut species, *Corylus americana*, that is
49 native to North America and resistant or highly tolerant of *A. anomala* infection, European
50 hazelnut is generally highly susceptible. In susceptible hosts, *A. anomala* infection results in the
51 formation of perennial cankers that girdle branches, culminating in tree death (Pinkerton 1995).
52 Current management practices are both costly and labour intensive relying on pruning and large
53 quantities of fungicides (Jeger et al. 2018). Further, it is documented that the *C. avellana* host
54 protection imparted through widely disseminated resistance (R) genes from *C. avellana* 'Gasaway'
55 in Oregon and other R genes mapped to the same linkage group, have been overcome in certain
56 regions (Jacobs et al. 2024a). Consequently, there is a pressing need to identify alternate strategies,
57 such as biocontrol, to reduce the impact of *A. anomala* on hazelnut cultivation.

58 A potential source of biocontrol agents is the native microbial community associated with
59 a plant species of interest. The plant microbiome is typically divided into three major regions: the

60 phyllosphere, representing the above-ground surface regions occupied by microbes; the
61 endosphere, representing the regions comprised of the plant's inner tissues; and the rhizosphere,
62 which refers to the thin layer of soil surrounding plant roots (Gupta et al. 2021; Santoyo 2022;
63 Zhang et al. 2021). The rhizosphere ecosystem is particularly complex (Jones and Hinsinger 2008)
64 laden with an exceptional diversity of life (Dlamini et al. 2022; Zhang et al. 2020). These plant
65 root-associated microbial communities have been referred to as the plant's second genome
66 (Berendsen et al. 2012), as they are capable of profoundly extending the plant's functional
67 potential (Bakker et al. 2013a). Notable examples of plant benefits conferred through these
68 associations include enhanced nutrient availability and improved tolerance to both biotic and
69 abiotic stress (Bakker et al. 2013b; Hakim et al. 2021; Pantigoso et al. 2022).

70 Importantly, rhizosphere microbial populations can be influenced by both the plant
71 genotype and its disease state (Liu et al. 2019; Liu et al. 2021; Liu et al. 2023a). Though conflicting
72 evidence has been reported (Fitzpatrick et al. 2018), increasing host plant phylogenetic distance
73 has been associated with less similar bacterial rhizosphere composition (Bouffaud et al. 2014; Lei
74 et al. 2019; Liu et al. 2023b), while two genotypes of the same plant species can possess similar
75 but distinguishable microbial populations (Peiffer et al. 2013). Likewise, domestication has been
76 found to influence microbiome assembly and metabolic functions (Yue et al. 2023).

77 At the same time, rhizosphere microbial communities may be modified based on plant root
78 secretions, with plants potentially recruiting and stimulating disease suppressive microbial taxa in
79 response to pathogens as a means of improving disease outcomes (Liu et al. 2023a). Rhizosphere
80 microbes may mitigate plant disease through antagonistic microbe-microbe interactions (Hassani
81 et al. 2018), priming of the plant immune system via induced systemic resistance (ISR) (Yu et al.
82 2022), and enhanced nutrient acquisition (Dordas 2008; Dotaniya and Meena 2015). Microbes that

83 exhibit these properties may therefore prove useful in disease management, through serving as
84 biopesticides, enhancing systemic plant disease tolerance through eliciting ISR, or by bolstering
85 overall plant vigour through facilitating nutrient acquisition. The rhizosphere microbiome is
86 therefore worth examining as a promising reservoir of disease attenuating agents, and
87 characterizing interactions between plant roots and their surrounding organisms has demonstrated
88 extensive promise for the improvement of economically valuable crops (Orozco-Mosqueda et al.
89 2022).

90 Unfortunately, the rhizosphere of woody perennial plants remains understudied relative to
91 annual crops. Despite the relative paucity of research in this area, the diverse utility of woody
92 perennial associated rhizosphere microbes has been validated by numerous studies. For example,
93 phosphate solubilizing microbes with plant growth promoting potential have been reported in the
94 peach rhizosphere (Li et al. 2025), highlighting the prospect of leveraging rhizosphere microbial
95 communities to enhance woody perennial vigour. In addition, the promise of certain walnut-
96 associated plant growth-promoting rhizobacteria (PGPR) for enhancing drought tolerance (Lotfi
97 et al. 2022) illustrates the abiotic stress ameliorating potential of microbes in the woody perennial
98 rhizosphere. Further, examples of the capacity of rhizosphere microbes to aid in combating biotic
99 stress have been reported for woody perennial crops including apple (Berdeni et al. 2018;
100 Derikvand et al. 2023), pear (Zhang et al. 2023), plum (Ali et al. 2018), and citrus (Ezrari et al.
101 2021). Collectively, these studies suggest woody perennial rhizosphere microbes may aid in
102 addressing several significant challenges facing woody perennial cultivation.

103 In the current study, shotgun metagenomics was used to investigate the rhizosphere
104 microbiome of North American grown hazelnut plants. To investigate the effect of genotype and
105 disease resistant phenotypes, samples were collected from an orchard infected with *A. anomala*

106 and were taken from the rhizospheres of native *C. americana* plants and *C. avellana* genotypes
107 that are resistant or susceptible to *A. anomala* infection. By gaining insight into the taxonomic and
108 functional features of hazelnut trees, this study broadens the scope of available genomic
109 information relevant to hazelnut improvement, including for disease management, and may help
110 guide future identification of biocontrol agents.
111

112 **RESULTS**

113 **Hazelnut rhizosphere sampling**

114 Rhizosphere samples were collected from 15 hazelnut trees situated at Rutgers University Hort
115 Farm 3, East Brunswick, New Jersey, USA, in October 2022. Five samples were collected from
116 each of the following tree types: native *C. americana* plants (henceforth referred to as "native"),
117 *C. avellana* resistant to *A. anomala* (henceforth referred to as "resistant), and susceptible *C.*
118 *avellana* (henceforth referred to as "susceptible"). The *C. americana* plants were derived from
119 open pollinated seeds obtained from wild plants in Dearborn, Michigan, whereas the *C. avellana*
120 plants were the product of a controlled cross of a H4AR21P05 (Jacobs et al. 2024b) female (open
121 pollinated seed from Warsaw, Poland) with a OSU 474.084 ('Lewis' x 'Tonda di Giffoni') x OSU
122 540.084 (a full sibling of 'Sacajawea') male pollen source, obtained from Shawn Mehlenbacher
123 of Oregon State University. These *C. avellana* plants were expected to segregate for a resistance
124 (R) gene originating from Poland (Capik et al., 2013). The two groups of *C. avellana* trees used
125 for this study, therefore, represent full siblings with the resistant group expressing no signs or
126 symptoms of disease and the susceptible expressing obvious signs of infection with pronounced
127 cankers and stem dieback predicated on segregation of the major R gene. At the time of collection,
128 the trees were ~6 years of age and have maintained consistent disease phenotypes for ~8 years as

129 of 2024. All rhizosphere samples were collected from soils adjacent to tree roots, at a depth of ~ 6
130 inches and a radius of ~ 6 inches from the trunk of the tree. For comparison, five bulk soil samples
131 (not near tree roots) were also collected from a depth of ~ 6 inches around the orchard; however,
132 the DNA isolation from one bulk soil sample failed, leaving us with four bulk soil samples.
133
134 **Metagenomic sequencing and assembly statistics**
135 Illumina 150 bp paired-end sequencing was used to characterize the microbial community of each
136 of the soil samples, generating between 35,138,424 and 118,478,008 paired-end reads per sample
137 (**Table S1**), of which between 31,340,823 and 113,588,930 survived quality control (**Table S1**).
138 Metagenome assembly using MEGAHIT resulted in assemblies of 544 Mb to 4007 Mb in size,
139 with N50 values between 446 kb and 2260 kb (**Table S1**). When limiting the metagenomes to
140 contigs of at least 0.5 kb in size, the assemblies averaged 612 Mb and contained an average of
141 768,075 contigs (**Table S1**). Likewise, when limiting the metagenomes to contigs of at least 1 kb
142 in size, the assemblies averaged 187 Mb and contained an average of 115,156 contigs (**Table S1**).
143
144 **Taxonomic characterization of the hazelnut rhizosphere**
145 Initially, the community composition of each rhizosphere and bulk soil sample was evaluated
146 based on the raw Illumina reads using Kraken2 and Bracken, with a database consisting of the
147 bacteria, archaea, fungi, and virus reference libraries. However, the rate of classification by
148 Kraken2 was low, with just 0.80% to 1.77% of reads assigned a taxonomy (**Table S2**).
149 Consequently, we instead used MMSeqs2 with the UniRef90 database, to taxonomically classify
150 the assembled contigs (minimum contig size of 0.5 kb); using this approach, contigs encompassing
151 between 6% and 31% of reads were assigned a taxonomy (**Table S2**). Overall, the metagenomes

152 were dominated by bacteria, with 82% to 96% of reads mapping to the classified contigs
153 corresponding to bacteria, compared to 1.0% to 9.5% and 0.3% to 3.8% for archaea and
154 eukaryotes, respectively.

155 Alpha diversity (Shannon diversity index and Simpson diversity index [1-D]) was
156 calculated from the MMSeqs2 output (**Figures 1A, 1B**). No statistically significant differences
157 were observed between sample groups using either of the diversity measures. However, both
158 diversity metrics displayed a trend of the bulk soil samples having lower diversity than the
159 rhizosphere samples; indeed, statistically significant differences were detected for both diversity
160 metrics when comparing bulk soil versus all rhizosphere samples grouped as a single treatment
161 (Kruskal-Wallis p-value < 0.05 for both metrics). In addition, although not statistically significant,
162 there appeared to be greater between-replicate variance in the diversity metrics for the non-native
163 *C. avellana* compared to native *C. americana* samples, perhaps suggesting that the rhizosphere
164 microbial community of the non-native plants was less stably assembled than that of the native
165 plants.

166 Beta diversity was calculated at the species level using Bray-Curtis dissimilarity (**Figure**
167 **1C**). Statistically significant differences (PERMANOVA p-value < 0.001) in beta diversity were
168 observed between the control and each of the three rhizosphere sample groups, providing support
169 that the rhizosphere samples were correctly collected and were reflective of the rhizosphere
170 community. However, no significant differences were observed between the native, resistant, and
171 susceptible rhizosphere samples, suggesting that plant genotype or disease state had little to no
172 impact on the rhizosphere microbiome at a global level.

173 To ensure that the diversity metrics were not being skewed by differences in read depth,
174 the sequencing reads were subsampled to achieve equivalent read numbers (following QC), after

175 which metagenomes were reassembled and MMSeqs2 rerun. The alpha and beta diversity metrics
176 were then recalculated from these data. This process produced qualitatively similar results for the
177 alpha and beta diversity metrics (**Figure S1**), indicating that the observed diversity values were
178 not heavily skewed by differences in read counts between samples.
179
180 **Differentially abundant taxa**
181 The relative abundances of major taxa were investigated across samples at the phylum and genus
182 levels (**Figures 2 and 3**). Initial, qualitative examination of the data revealed that all samples were
183 dominated by the bacterial phyla *Actinomycetota*, *Pseudomonadota*, and *Acidobacteriota* (**Figure**
184 **2A**). At the genus level, the three most abundant taxa were the common soil bacteria
185 *Bradyrhizobium*, *Gaiella*, and *Nocardioides* (**Figure 3A**). Although the archaea represented only
186 a minority of the metagenomes, the archaeal component was dominated by the phylum
187 *Thermoproteota* (syn. *Nitrosophaerota*) (**Figure 2B**), driven by the abundance of the genera
188 *Nitrososphaera* and "*Candidatus* Nitrosocosmicus" (**Figure 3B**). Lastly, examination of the
189 eukaryotic taxa revealed the phylum Basidiomycota was substantially enriched in the rhizosphere
190 samples relative to the bulk soil control, while the phylum Ascomycota also appeared somewhat
191 enriched in many of the rhizosphere samples (**Figure 2C**). The differential abundance of the
192 phylum Basidiomycota was driven mostly by the genera *Hebeloma*, *Laccaria*, *Galerina*,
193 *Scleroderma*, and *Pisolithus* while the differential abundance of the phylum Ascomycota was
194 driven mostly by the genus *Morchella* and to a lesser extent the genus *Terfezia* (**Figure 3C**). It is
195 important to note, however, that some unexpected eukaryotic taxa were identified in relatively
196 high abundance, such as the shark genus *Chiloscyllium* (**Figure 3C**). This may be the result of
197 poor taxonomic classification of the eukaryotic contigs and/or the overall low abundance of

198 eukaryotes in the data. Regardless, it does suggest that caution should be taken in interpreting the
199 abundance data for the eukaryotic taxa.

200 Following qualitative assessment of the abundance data, ANCOMBC2 was used for
201 quantitative assessment of differential abundances of the taxa accounting for at least 1% of the
202 overall relative abundances of the communities. At the phylum level, the eukaryotic phylum
203 Basidiomycota and the bacterial phylum "*Candidatus* Rokuibacteriota" appeared enriched in all
204 three rhizosphere groups relative to the bulk soil controls with (log2[fold change] ≥ 3.9 and 2.3,
205 for Basidiomycota and "*Candidatus* Rokuibacteriota", respectively; **Figure 2A**). On the other
206 hand, the bacterial phylum *Verrucomicrobiota* appeared underrepresented specifically in the
207 rhizosphere communities of the "resistant" *C. avellana* plants relative to the bulk soil controls
208 (log2[fold change] of -1.2; **Figure 2A**). At the genus level, the three rhizosphere groups appeared
209 depleted in the bacterial genus *Trebonia* relative to the bulk soil control (**Figure 3A**). Compared
210 to the bulk soil control, the resistant and susceptible *C. avellana* samples (but not the *C. americana*
211 samples) both had an underrepresentation of the bacterial genera *Actinospica* (log2[fold change]
212 ≤ -1.4), *Occallatibacter* (log2[fold change] ≤ -2.8) and "*Candidatus* Sulfotelmatobacter"
213 (log2[fold change] ≤ -2.9), while the bacterial genus *Rhizobacter* appeared enriched (log2[fold
214 change] ≥ 1.5). The resistant *C. avellana* samples also appeared enriched in the bacterial genus
215 *Illumatobacter* relative to the bulk soil control. Lastly, the bacterial genus *Microbacterium* was
216 enriched in the resistant *C. avellana* samples relative to the native variety (log2[fold change] of
217 2.0). *Microbacterium* also visually appeared to be enriched in the susceptible *C. avellana*
218 compared to the native variety although this difference was not statistically significant.

219

220

221 **Functional overview of the metagenomes**

222 DRAM was used for functional annotation of all contigs of at least 1 kb in length, and the relative
223 abundance of genes assigned KEGG annotations were used to construct a PCoA plot using Bray-
224 Curtis dissimilarities as a general overview of the functional differentiation of each sample (**Figure**
225 **4**). Although global differences between samples were detected (PERMANOVA p-value of
226 0.031), no statistically significant differences were noted for any of the pairwise comparisons
227 between sample groups. However, although not statistically significant, there did appear to be a
228 trend towards the native *C. americana* and resistant *C. avellana* samples grouping together and
229 separating from the sensitive *C. avellana* and bulk soil control. Likewise, no clear differences were
230 noted between sample types when comparing the presence of various functions and pathways
231 related to carbohydrate metabolism, methanogenesis and methanotrophy, nitrogen metabolism,
232 short-chain fatty acid and alcohol conversions, and sulfur metabolism (**Figure S2**). Overall, these
233 results indicate that there was little functional differentiation between the sample types at a global
234 level.

235 In addition, prokaryotic biosynthetic gene clusters (BGCs) were annotated in all
236 metagenome assemblies (limited to contigs of at least 0.5 kb) using the program antiSMASH. BiG-
237 SCAPE was then used to group the antiSMASH annotations based on the class and predicted
238 products of the BGCs (**Figure 5**). The distribution of BGCs across samples was largely similar,
239 regardless of the sample group, with BGC classes associated with nonribosomal peptide
240 synthetases (NRPS), ribosomally synthesized and post-translationally modified peptides (RiPPs),
241 and terpenes generally present with the highest relative abundance.

242

243

244 **Reconstruction and characterization of metagenome-assembled genomes**

245 Following dereplication using an average nucleotide identity (ANI) threshold of 99%, 45 high-
246 quality (completeness ≥ 70%, contamination ≤ 10%) metagenome-assembled genomes (MAGs)
247 were constructed from the dataset and taxonomically categorized with GTDB-Tk, including 41
248 bacterial and 4 archaeal MAGs (**Figure 6, Table S3**). Interestingly, only one of the 45 MAGs
249 could be taxonomically classified as the species level when using the Genome Taxonomy Database
250 Toolkit (GTDB-Tk) with database R220, while an additional nine were classified to the genus
251 level. The four archaeal MAGs represent four distinct species from three genera within the family
252 *Nitrososphaeraceae* (phylum *Thermoproteota*). On the other hand, nine phyla are represented
253 amongst the 41 bacterial MAGs, with the majority of MAGs belonging to the phyla
254 *Actinomycetota* (21 MAGs), *Pseudomonadota* (9 MAGs), and *Acidobacteriota* (6 MAGs). MAGs
255 were functionally annotated with DRAM, and a summary of the results are provided as **Figure S3**.
256 In addition, antiSMASH and BiG-SCAPE were used to detect and summarize the abundance of
257 BGCs in the MAGs, and these results are summarized in **Figure S4**.

258

259 **DISCUSSION**

260 **The hazelnut rhizosphere microbiome showed only minor differences compared to bulk soil**

261 Previous studies examining bacterial community structure in the roots of the woody plants
262 (*Quercus*, *Populus*, and *Pinus*), found that bacterial community structure was shaped more
263 strongly by host tree species than by soil origin (Bonito et al. 2014). We therefore expected to see
264 differences between the microbial community of the rhizosphere samples compared to the bulk
265 soil samples. As expected, the bulk soil samples were clearly delineated from the rhizosphere
266 samples based on the alpha and beta diversity measures. This differentiation appeared to be mainly

267 driven by changes in frequency of low abundance taxa as we observed few differences in the
268 relative abundances of the primary taxa (those with relative abundances ≥ 1%). However, the
269 current study examined only a single time point. Considering that another study observed that the
270 prokaryotic component of the maize rhizosphere only differed from bulk soil at specific stages of
271 plant development (Wattenburger et al. 2019), it may be that sampling at a different time of year,
272 or sampling deeper roots, would reveal more dramatic changes in the hazelnut rhizosphere
273 microbial community structure than observed here.

274 Few differences were observed between the microbial communities of the different
275 hazelnut genotypes, contrary to our expectation (Lopes et al. 2023). Likewise, we observed little
276 difference between *C. avellana* plants that were or were not infected with *A. anomala*, despite
277 previous studies observing that foliar pathogens can indirectly impact rhizosphere microbial
278 communities in ways that could potentially have positive impacts on plant disease tolerance
279 (Berendsen et al. 2018; Jiang et al. 2023; Luo et al., 2022; Yang et al. 2020). While these results
280 could suggest that hazelnut genotype and disease status have little impact on the rhizosphere
281 microbiome, it may also be that differences would be more pronounced at other times of the year,
282 or that deeper sequencing and/or taxonomic classification of a higher portion of the contigs would
283 reveal additional differences missed here.

284

285 **Composition of the hazelnut microbial community**

286 We found that the fungal phylum Basidiomycota was enriched in all rhizosphere samples relative
287 to bulk soil. Likewise, the fungal phyla Ascomycota was slightly enriched in the rhizosphere
288 samples, although this enrichment was not statistically significant. Interestingly, a separate study
289 reported Ascomycota, Basidiomycota, and Mortierellomycota as the dominant fungal phyla in the

290 rhizosphere of hazelnut varieties grown in Beijing, China (Ma et al. 2021). Similarly, the phyla
291 Basidiomycota and Ascomycota were the dominant fungal phyla in the rhizosphere of the
292 deciduous shrub *Paeonia ludlowii*, with Basidiomycota being the most dominant in the autumn
293 (Qiao et al. 2023). Overall, the consistency in these results provides support that our rhizosphere
294 samples accurately capture the hazelnut rhizosphere microbiome.

295 Although there is limited data on the effects of bacteria on hazelnut tree health and growth,
296 one study reported that inoculation of *C. avellana* seedlings with the bacteria *Pseudomonas putida*,
297 *B. subtilis*, and *Enterobacter cloacae* can improve growth (Rostamikia et al. 2017). Therefore, we
298 wished to use our metagenomics data to help identify microbes in the hazelnut rhizosphere
299 microbiome that could potentially be targets to develop into biocontrol agents to limit the impact
300 of *A. anomala* infection. To this end, we focused on the microbes that were either enriched or
301 depleted in the hazelnut microbiome. One taxon of particular interest based on the relative and
302 differential abundance data was the bacterial phylum "*Candidatus* Rokuibacteriota", which was
303 enriched in all three rhizosphere groups relative to bulk soil. "*Candidatus* Rokuibacteriota" have
304 large genomes with high GC content, with the capacity for multifaceted mixotrophic metabolism
305 (Becraft et al. 2017). Bacteria from this phylum have also been reported to encode numerous
306 biosynthetic loci in their genomes (Sharrar et al. 2020). Consequently, members of this phylum
307 exhibit characteristics of relevance for biocontrol applications, and we suggest that their utility
308 should be explored within this context.

309 On the other hand, the bacterial genera *Actinospica*, *Occallatibacter*, and "*Candidatus*
310 Sulfotelmatobacter" were depleted in the susceptible and tolerant varieties of *C. avellana* relative
311 to bulk soil, unlike the native *C. americana* variety. *Actinospica* may be of particular note for *A.*
312 *anomala* disease management, as there is an ongoing interest in the efficacy of acidophilic

313 actinomycetes as biocontrol agents against phytopathogenic fungi (Poomthongdee et al. 2015).
314 Supplementing the abundance of this genus in the *C. avellana* microbiome may therefore be a
315 strategy worth exploring for *A. anomala* disease management.

316 In terms of eukaryotic microbes, associations with mycorrhizal fungi have been shown to
317 enhance disease tolerance in woody perennials (Dong et al. 2021; Kebert et al. 2022), and a variety
318 of additional benefits have been described for mycorrhizal associated hazelnut trees. In *C.*
319 *avellana*, association with the ectomycorrhizal forming fungus *Tuber melanosporum* was reported
320 to regulate important plant defense genes, which may favourably impact the host plant's response
321 to stress (Sillo et al. 2022). Inoculation of hybrid hazel (*C. heterophylla* x *C. avellana*) seedlings
322 with the ectomycorrhizal fungus *Scleroderma bovista* was reported to promote growth, enhancing
323 photosynthetic efficiency and total plant weight (Cheng et al. 2024). In addition, inoculation with
324 the arbuscular mycorrhizal fungus *Glomus iranicum* var. *tenuihypharum* was found to increase the
325 number of female flowers and overall yield in the Tonda di Giffoni variety of *C. avellana* by 60%
326 and 38%, respectively, relative to the uninoculated control (Luciani et al. 2019). In our study, the
327 fungal genera *Hebeloma*, *Galerina*, *Laccaria*, *Morchella*, *Pisolithus*, and *Scleroderma* appeared
328 enriched in the three groups of rhizosphere samples, relative to the control group; however, as the
329 relative abundances of these taxa were < 1%, the differences in their abundances was not tested
330 using ANCOMBC2. Isolates of species from these fungal taxa from the hazelnut rhizosphere may
331 therefore represent interesting candidates to explore for plant growth promotion and/or biocontrol
332 against *A. anomala* in North America.

333

334 **Primary metabolism of the hazelnut rhizosphere microbiome**

335 Rhizosphere microbes play important roles in nutrient cycling and availability (Thepbandit and

336 Athinuwat 2024) and consequently, they can impact plant nutrition and thus disease tolerance. For
337 example, nitrogen availability can impact both physical and biochemical defence mechanisms in
338 plants, yet the consequences of enhanced endogenous nitrogen can be difficult to anticipate, as
339 they may be favourable or detrimental to plant pathogen tolerance depending on context (Sun et
340 al. 2020). In our study, global differences in the KEGG metabolic annotations (PERMANOVA p-
341 value of 0.031) were observed between samples, however no pairwise differences were detected
342 between sample groups.

343 Pathways involved in nitrogen metabolism were well represented across most samples
344 including ammonia oxidation, conversion of nitrate to nitrite, nitrite to nitrate, nitrite to nitric
345 oxide, and nitric oxide to nitrous oxide. Though less common, some samples possessed the
346 capacity for nitrite reduction to ammonia as observed in Bulk soil 1, Bulk soil 2, Native 3,
347 Susceptible 1, Susceptible 2, and Susceptible 4 samples. As nitrate serves as the major source of
348 nitrogen for most land plants in aerobic soils (Ho and Tsay 2010), the presence of pathways
349 involved in the production of nitrate across samples highlights the capacity of microbes within
350 these systems to facilitate the production of bioavailable nitrogen for hazelnut. Bioavailable sulfur
351 can also have drastic impacts on plant disease outcomes. For example, inorganic sulfate salts can
352 significantly enhance the resistance of plants to certain fungal pathogens, through a process
353 deemed sulfur-induced resistance (SIR) (Künstler et al. 2020). Here, pathways responsible for the
354 conversion of thiosulfate to sulfate were well represented across all samples besides the
355 Susceptible 3 sample. As both bioavailable nitrogenous and sulfur-containing compounds have
356 been demonstrated to alter plant disease tolerance (Bloem et al. 2015; Mur et al. 2017) the
357 application of certain microbial communities that alter the abundance of bioavailable forms of
358 these compounds within the soil may be explored as an alternative means of broadly improving

359 plant health.

360 Many of the MAGs generated in this study, particularly those within the orders *Gaiellales*
361 and *Hyphomicrobiales* (syn. *Rhizobiales*), encoded pathways involved in the conversion of nitrite
362 to nitric oxide (NO). NO can be generated endogenously in plants and performs important
363 functions in various physiological responses and developmental stages (Hancock 2020; Sun et al.
364 2021), with roles in plant tolerance to abiotic and biotic stress (Fancy et al. 2017, 201; Mur et al.
365 2017). Exogenous application of NO, through the use of NO donors, has been shown to improve
366 plant disease tolerance in several instances (Nasir et al. 2020; Khan et al. 2021; Bakhoum et al.
367 2023). Furthermore, studies suggest that leveraging NO-producing organisms to enhance disease
368 tolerance in plants is a promising avenue to explore. For example, a study examining tomato
369 infected with *Ralstonia solanacearum* found that *Pseudomonas fluorescens* strains overproducing
370 NO displayed better biocontrol efficacy than those that don't overproduce NO (Wang et al. 2005).
371 Consequently, it would be interesting to isolate diverse strains from promising genera within the
372 *Gaiellales* and *Hyphomicrobiales* orders, which we found commonly encode the pathways for NO
373 production, and assess them for their impact on hazelnut disease tolerance. Of particularly interest
374 would be isolates that additionally have the potential to convert thiosulfate to sulfate.

375

376 **Secondary metabolism of the hazelnut rhizosphere microbiome**

377 Soil microbes represent a rich source of secondary metabolites (Sharrar et al. 2020) that perform
378 diverse functions in ecological systems and can mediate symbioses between microbes and plants
379 in certain contexts (Demain and Fang 2000) and ameliorate biotic stress in plants (Ruparelia et al.
380 2022). Analyzing the biosynthetic gene clusters (BGCs) involved in the production of secondary
381 metabolites within the hazelnut rhizosphere, therefore, provides an opportunity to identify

382 compounds and microbial taxa that can be screened as biological control agents in hazelnut.

383 In our study, no substantial differences in the relative abundance of specific BGC classes
384 were evident between conditions, although all conditions had an abundance of BGCs encoding the
385 production of non-ribosomal peptides (NRPs), ribosomally synthesized and post-translationally
386 modified peptides (RiPPs), and terpenes. The production of secondary metabolites of these classes
387 has repeatedly been shown to contribute to the biocontrol potential of plant growth-promoting
388 rhizobacteria (PGPRs). For example, *Bacillus* species produce NRPs that can serve as biocontrol
389 agents, such as iturin, surfactin and fengycin (Ranjan et al. 2023). Likewise, species of the fungal
390 genus *Trichoderma* have demonstrated potential as biocontrol agents (Sood et al. 2020), which
391 could relate to the diversity of terpenoids and complex terpenes produced by these organisms (Bai
392 et al. 2022; Lee et al. 2016).

393 Many of the MAGs assembled in this study have the genetic potential to produce diverse
394 secondary metabolites. One such example is MAG-30, classified as belonging to the species
395 "*Lysobacter yananisis*". Species of the genus *Lysobacter* have potential as biocontrol agents
396 (Kilic-Ekici and Yuen 2003; Puopolo et al. 2014), and they produce a range of antibiotics active
397 against numerous plant pathogens (Gómez Expósito et al. 2015; Hayward et al. 2010). Likewise,
398 our *Lysobacter* MAG has the genetic potential to produce various secondary metabolites of
399 relevance for biocontrol, including NRPs, lantipeptides, polyketides, and RiPPs. Another MAG
400 with high biosynthetic potential is MAG-07, classified as belonging to the genus *Actinospica*.
401 Species of this genus have been isolated from diverse ecosystems including forest soils (Kusuma
402 et al. 2022; Cavaletti et al. 2006), and studies suggest that members of this genus have strong
403 biocontrol potential (Qi et al. 2019; Rodriguez-Mena et al. 2022). Indeed, members of the genus
404 *Actinospica* have high genetic potential to produce a wide array of secondary metabolites (Majer

405 et al. 2021). Likewise, our *Actinospica* MAG contains several genomic regions potentially
406 involved in the production of NRPs, lantipeptides, RIPPs, polyketides, and terpenes. Considering
407 these results, it would be interesting to isolate strains of the genera *Lysobacter* and *Actinospica*
408 from hazelnut rhizosphere soils and investigate their potential to serve as biocontrol strains and
409 reduce the susceptibility of hazelnut to *A. anomala* infection.
410

411 **Conclusions**

412 The co-evolution of plants and their resident microbial communities has resulted in a complex
413 dynamic where the microbial genetic complement can drastically impact important plant features.
414 Soil microbes participate in important biogeochemical cycles that impact plant nutrient
415 acquisition, while plant-associated microbes can also influence plant immunity. Here,
416 metagenomics was used to examine the microbial communities of three hazelnut rhizosphere
417 sample groups obtained from trees that displayed differing levels of resistance to the pathogen *A.*
418 *anomala*: *C. americana* (resistant), *C. avellana* (susceptible) and *C. avellana* (resistant). While the
419 rhizosphere samples were differentiated from the bulk soil samples, little taxonomic or functional
420 variation was seen between the different rhizosphere groups. A total of 45 dereplicated, high-
421 quality MAGs were generated, many of which carried multiple BGCs. This included two MAGs
422 representing organisms from the bacterial genera *Actinospica* and *Lysobacter* that have previously
423 been identified as potential biocontrol agents. This study serves to inform future efforts aimed at
424 leveraging hazelnut-associated microbes toward the improvement of diverse hazelnut features
425 including disease outcomes, identifying promising candidate taxa that could be isolated and
426 screened for their capacity to manage *A. anomala* infection. In addition, this study provides
427 insights into the taxonomic diversity and functional potential of the rhizosphere microbial

428 communities of hazelnut, expanding our understanding of the rhizosphere microbiome of woody
429 perennials.
430
431 **METHODS**

432 **Soil sample collection**

433 Bulk soil and rhizosphere samples were collected from Hort Farm 3, 67 Ryders Lane, East
434 Brunswick, NJ 08816, between 1:00 PM and 4:00 PM on 19 October 2022. Soils were collected
435 using a small shovel that was sterilized with 70% ethanol before each sample collection, and
436 transferred to sterile 50 mL tubes. Soils from highly tolerant *C. americana* trees were collected
437 from row 1 of the farm. Soils from *C. avellana* trees collected from row 3 were divided into two
438 groups segregating for disease resistance, designated resistant and susceptible, based on the
439 presence or absence of pronounced *A. anomala* cankers. Five soil samples were collected for each
440 of the three hazelnut varieties; samples were collected at a depth of approximately 15 cm,
441 approximately 15 cm away from the trunk of the tree. In addition, five bulk soil samples were
442 collected at a depth of approximately 15 cm from five sites around the periphery of the hazelnut
443 orchard.
444

445 **DNA isolation and sequencing**

446 Approximately one hour after sample collection was complete, ~0.42 g subsamples of soil were
447 taken from each soil sample. DNA extraction was performed using a Qiagen DNeasy PowerSoil
448 Pro Kit, according to the manufacturer's instructions. One of the bulk soil samples was omitted
449 from downstream analysis due to failure of the DNA extraction. All other DNA samples were
450 subsequently refrigerated until they were shipped to Génome Québec (Montréal, Quebec, Canada)

451 for library preparation and Illumina sequencing. For samples B2, B3, B5, R1P5, R1P9, R1P14,
452 R3P3, R3P15, R3P20, R3P9-, R3P10-, R3P12- (**Table 1**), library preparation was performed using
453 the NxSeq® AmpFREE Low DNA Library Preparation Kit (Lucigen) using the Xp protocol, as
454 suggested by the manufacturer. These samples were sequenced using 150-bp paired-end
455 technology on an Illumina NovaSeq 6000 instrument. For samples B4, R1P1, R1P18, R3P5,
456 R3P11, R3P14-, R3P18- (**Table 1**), library preparation was performed using the (Illumina®) DNA
457 PCR-Free Prep, Tagmentation Kit following the manufacturer's recommendations. These samples
458 were likewise sequenced using 150-bp paired-end technology, but on an Illumina NovaSeq X Plus
459 instrument.
460
461 **Taxonomic classification of the raw Illumina reads**
462 Illumina reads were taxonomically classified using Kraken (v2.1.3) (Wood et al. 2019) using a
463 database consisting of the bacteria, archaea, fungi, and virus reference libraries, and post-processed
464 using Bracken (v2.7) (Lu et al. 2017). Alpha diversity and beta diversity measurements were
465 determined based on the species-level output of Bracken. Diversity measurements were
466 determined, analyzed, and visualized in R (v4.5.1) (R Core Team 2025) using tidyverse (v2.0.0)
467 (Wickham et al. 2019), dplyr (v1.1.4) (Wickham et al. 2018) , phyloseq (v1.52.0) (McMurdie and
468 Holmes 2013), stats (v4.5.1) (R Core Team 2025), ggpubr (v0.6.1) (Kassambara 2025), vegan
469 (v2.7.1) (Oksanen et al. 2024), pairwiseAdonis (v0.4.1) (Martinez Arbizu 2017), ggplot2 (v4.0.0)
470 (Wickham 2009), and patchwork (v1.3.2) (Pedersen 2019) packages. KronaTools (v2.8) (Ondov
471 et al. 2011) was used for generation of krona plots.
472
473

474 **Metagenome assembly and binning**

475 Illumina reads were filtered using BBduk (v39.06) (Bushnell 2014) and trimmed using
476 Trimmomatic (v0.39) (Bolger et al. 2014) with the parameters: LEADING:3 TRAILING:3
477 SLIDINGWINDOW:4:15 MINLEN:36. Following trimming, metagenomes were assembled
478 using MEGAHIT (v1.2.9) (Li et al. 2015) with the "presets" option set to "meta-large".
479 Metagenome assembly statistics were calculated using the stats.sh script of BBMap (v37.36)
480 (Bushnell 2014). In addition, to confirm that the alpha and beta diversity metrics were not
481 confounded by differences in sequencing depth, seqtk (v1.3) (https://github.com/lh3/seqtk) was
482 used to filter the trimmed reads to obtain a subset corresponding to 90% of the number of reads
483 from the sample with the fewest reads. These reduced read sets were then used for metagenome
484 assembly using MEGAHIT with the "presets" option set to "meta-large".

485

486 **Assembly of metagenome-assembled genomes**

487 Prior to binning, contigs less than 1500 bp were discarded using pullseq (v1.0.2)
488 (https://github.com/bcthomas/pullseq). Next, an all-against-all mapping of the Illumina reads
489 against each metagenome was performed using bowtie2 (v2.4.5) (Langmead and Salzberg 2012)
490 and sorted using samtools (v1.15.1) (Li et al. 2009). Binning was then performed independently
491 for each sample using MetaBAT2 (v2.14) (Kang et al. 2019), CONCOCT (v1.1.0) (Alneberg et
492 al. 2014), MaxBin2 (v2.2.7) (Wu et al. 2016), and SemiBin2 (v2.1.0) (Pan et al. 2023). From each
493 of the metagenomes, an optimized set of MAGs was produced using DAS_Tool (v1.1.4) (Sieber
494 et al. 2018) and the output of the four binning algorithms. In addition, bins were generated with
495 VAMB (v4.1.3) (Nissen et al. 2021, 20), using all metagenomes and with read mapping performed
496 using minimap2 (v2.24-r1122) (Li 2018). Finally, a non-redundant set of high-quality MAGs (>

497 70% completeness; < 10% contamination) was generated from all the produced MAGs using dRep
498 (v3.4.1) (Olm et al. 2017) and a secondary clustering threshold of 99%. The dependencies for dRep
499 included Mash (v2.3) (Ondov et al. 2016) MUMmer (v4.0.0rc1) (Kurtz et al. 2004), CheckM
500 (v1.2.2) (Parks et al. 2015), Prodigal (v2.6.3) (Hyatt et al. 2010), and pplacer (v1.1.alpha19)
501 (Matsen et al. 2010).
502
503 **Taxonomic classification of the assembled metagenomes**
504 Prior to taxonomic classification, contigs less than 500 bp were discarded using pullseq. Contigs
505 were taxonomically classified using MMSeqs2 (v0a6b8c) (Steinegger and Söding 2017) with the
506 UniRef90 database (downloaded 18 July 2024). Custom scripts were used to convert the MMSeqs2
507 output data into taxa abundance tables, with taxa abundances calculated as the sum of contig length
508 multiplied by contig sequencing depth for all contigs with a given taxonomic classification. Alpha
509 diversity and beta diversity metrics were determined, analyzed, and visualized in R using the
510 tidyverse, ggplot2, dplyr, phyloseq, stats, ggpubr, vegan, pairwiseAdonis, and patchwork
511 packages. The relative abundances of the taxa were visualized as bubble plots and stacked bar plots
512 with R's ggplot2, patchwork, and randomcoloR (v1.1.0.1) (Ammar 2019) packages. Lastly, the R
513 packages ANCOMBC2 (v2.10.1) (Lin and Peddada 2024) and microbiome (v1.30.0) (Lahti and
514 Shetty 2019) were used to identify statistically significant differences in taxa abundances for taxa
515 with a relative abundance of at least 1% in at least one sample. The relevant data from these
516 analyses were visualized in R using the ggplot2 and patchwork packages.
517
518 **Taxonomic classification of metagenome-assembled genomes**
519 MAGs were taxonomically classified using GTDB-Tk (v2.4.0) with the R220 database and the

520 classify_wf workflow (Chaumeil et al. 2020). To construct a phylogeny of the bacterial MAGs,
521 the identify function of GTDB-Tk was used to identify homologs of the bac120 gene set, following
522 which the align function of GTDB-Tk was used to align each marker set and then concatenate the
523 alignments. Lastly, the concatenated alignment was used to construct a maximum likelihood
524 phylogeny using IQ-TREE2 (v2.2.2.4) (Minh et al. 2020). First, ModelFinder (Kalyaanamoorthy
525 et al. 2017), was used to identify the best scoring model based on Bayesian information criterion
526 (BIC). Then, IQ-TREE2 was run using the best-scoring model (LG+F+R5) with branch support
527 assessed using the Shimodaira–Hasegawa-like approximate likelihood ratio test (SH-aLRT) and
528 ultrafast jackknife analysis with a subsampling proportion of 40%, with both metrics calculated
529 from 1,000 replicates. Phylogenies were visualized using iTOL (Letunic and Bork 2024).
530

531 **Characterization of the metabolic potential of the metagenomes and MAGs**

532 Prior to functional annotation, contigs less than 1000 bp were discarded from the metagenomes
533 using pullseq. Next, DRAM (v0.1.2) (Shaffer et al. 2020), as implemented on the KBase platform
534 (Arkin et al. 2018), was used to annotate all metagenomes and MAGs. For the metagenomes, the
535 KEGG annotations were extracted from the annotation file, and a Bray-Curtis distance matrix was
536 produced and visualized using a Principal Coordinate Analysis in R with the ggplot2, dplyr,
537 phyloseq, and patchwork packages. Statistical analyses were performed in R using the vegan and
538 pairwiseAdonis packages. Group specific functional differences were determined and visualized
539 using the dplyr, stats, dunn.test (v1.3.6) (Dinno 2024), and ggplot2 packages.

540 Prior to annotation of BGCs, contigs less than 500 bp were discarded from the
541 metagenomes using pullseq. BGCs were identified in the reduced metagenomes using antiSMASH
542 (v7.0) (Blin et al. 2023) with default parameters, after which BiG-SCAPE (v1.1.8) (Navarro-

543 Muñoz et al. 2020) was run with default parameters to examine BGC diversity across the
544 metagenomes. Likewise, BGCs were identified in the MAGs using antiSMASH and BiG-SCAPE.
545 The output files were processed and visualized as heatmaps in R using the dplyr, ggplot2 and
546 patchwork packages.
547
548 **Data availability**
549 All raw Illumina sequencing data, metagenome assemblies, and MAGs are available from the
550 National Center for Biotechnology Information (NCBI) under BioProject PRJNA1338491
551 Accessions for individual datasets are provided in **Table S3**. All code to repeat the analyses
552 described in this manuscript is available through GitHub (github.com/diCenzo-
553 Lab/016_2025_hazelnut_rhizosphere_metagenomics).
554
555 **ACKNOWLEDGEMENTS**
556 We thank Sharen Roland and other personnel at the Centre d'Expertise et de Services (CES) of
557 Génome Québec for the advice on sequencing strategies and for performing all the Illumina
558 sequencing reported in this study. We would also like to thank Rutgers University Department of
559 Plant Biology for providing access to their facilities for sample collection and preparation. This
560 work was also supported by the USDA-NIFA Hatch project NJ12171 through the New Jersey
561 Agricultural Experiment Station. This work was funded by the Natural Sciences and Engineering
562 Research Council of Canada (NSERC) through Discovery Grants to S.R. and G.C.D. and the
563 NSERC Collaborative Research and Training Experience Grant "Genome Editing for
564 Food Security and Environmental Sustainability" to S.R. This research was enabled, in part,
565 through computational resources provided by Compute Ontario (computeontario.ca) and the

566 Digital Research Alliance of Canada (alliancecan.ca).

567

568 **REFERENCES**

569 Ali, I., Sultan, T., Subhan, F., Haleem, K. S., Sultana, N., and Tauseef, I. 2018. PGPRs of plum
570 (*Prunus domestica*) rhizosphere enhance plant growth and antagonize fungal activity in
571 vitro. **Acta Agric. Scand. Sect. B — Soil Plant Sci.** 68:367–378.
572 https://doi.org/10.1080/09064710.2017.1410565.

573 Alneberg, J., Bjarnason, B. S., de Bruijn, I., Schirmer, M., Quick, J., Ijaz, U. Z., Lahti, L., Loman,
574 N. J., Andersson, A. F., and Quince, C. 2014. Binning metagenomic contigs by coverage and
575 composition. **Nat. Methods** 11:1144–1146. https://doi.org/10.1038/nmeth.3103.

576 Ammar, R. 2019. **randomcoloR: generate attractive random colors.** https://CRAN.R-
577 project.org/package=randomcoloR.

578 Arkin, A. P., Cottingham, R. W., Henry, C. S., Harris, N. L., Stevens, R. L., Maslov, S., Dehal, P.,
579 Ware, D., Perez, F., Canon, S., Sneddon, M. W., Henderson, M. L., Riehl, W. J., Murphy-
580 Olson, D., Chan, S. Y., Kamimura, R. T., Kumari, S., Drake, M. M., Brettin, T. S., Glass, E.
581 M., Chivian, D., Gunter, D., Weston, D. J., Allen, B. H., Baumohl, J., Best, A. A., Bowen,
582 B., Brenner, S. E., Bun, C. C., Chandonia, J.-M., Chia, J.-M., Colasanti, R., Conrad, N.,
583 Davis, J. J., Davison, B. H., DeJongh, M., Devoid, S., Dietrich, E., Dubchak, I., Edirisinghe,
584 J. N., Fang, G., Faria, J. P., Frybarger, P. M., Gerlach, W., Gerstein, M., Greiner, A.,
585 Gurtowski, J., Haun, H. L., He, F., Jain, R., Joachimiak, M. P., Keegan, K. P., Kondo, S.,
586 Kumar, V., Land, M. L., Meyer, F., Mills, M., Novichkov, P. S., Oh, T., Olsen, G. J., Olson,
587 R., Parrello, B., Pasternak, S., Pearson, E., Poon, S. S., Price, G. A., Ramakrishnan, S.,
588 Ranjan, P., Ronald, P. C., Schatz, M. C., Seaver, S. M. D., Shukla, M., Sutormin, R. A., Syed,

589 M. H., Thomason, J., Tintle, N. L., Wang, D., Xia, F., Yoo, H., Yoo, S., and Yu, D. 2018.
590 KBase: The United States Department of Energy Systems Biology Knowledgebase. **Nat.**
591 **Biotechnol.** 36:566–569. https://doi.org/10.1038/nbt.4163.
592 Bai, B., Liu, C., Zhang, C., He, X., Wang, H., Peng, W., and Zheng, C. 2022. *Trichoderma* species
593 from plant and soil: an excellent resource for biosynthesis of terpenoids with versatile
594 bioactivities. **J. Adv. Res.** 49:81–102. https://doi.org/10.1016/j.jare.2022.09.010.
595 Bakhoum, G. Sh., Sadak, M. Sh., and Thabet, M. S. 2023. Induction of tolerance in groundnut
596 plants against drought stress and *Cercospora* leaf spot disease with exogenous application
597 of arginine and sodium nitroprusside under field conditions. **J. Soil Sci. Plant Nutr.**
598 23:6612–6631. https://doi.org/10.1007/s42729-023-01514-x.
599 Bakker, P. A. H. M., Berendsen, R. L., Doornbos, R. F., Wintermans, P. C. A., and Pieterse, C. M.
600 J. 2013a. The rhizosphere revisited: root microbiomics. **Front. Plant Sci.** 4.
601 https://doi.org/10.3389/fpls.2013.00165.
602 Bakker, P. A. H. M., Doornbos, R. F., Zamioudis, C., Berendsen, R. L., and Pieterse, C. M. J.
603 2013b. Induced systemic resistance and the rhizosphere microbiome. **Plant Pathol. J.**
604 29:136–143. https://doi.org/10.5423/PPJ.SI.07.2012.0111.
605 Becraft, E. D., Woyke, T., Jarett, J., Ivanova, N., Godoy-Vitorino, F., Poulton, N., Brown, J. M.,
606 Brown, J., Lau, M. C. Y., Onstott, T., Eisen, J. A., Moser, D., and Stepanauskas, R. 2017.
607 Rokubacteria: genomic giants among the uncultured bacterial phyla. **Front. Microbiol.** 8.
608 https://doi.org/10.3389/fmicb.2017.02264.
609 Berdeni, D., Cotton, T. E. A., Daniell, T. J., Bidartondo, M. I., Cameron, D. D., and Evans, K. L.
610 2018. The effects of arbuscular mycorrhizal fungal colonization on nutrient status, growth,
611 productivity, and canker resistance of apple (*Malus pumila*). **Front. Microbiol.** 9:1461.

612 https://doi.org/10.3389/fmicb.2018.01461.
613 Berendsen, R. L., Pieterse, C. M. J., and Bakker, P. A. H. M. 2012. The rhizosphere microbiome
614 and plant health. **Trends Plant Sci.** 17:478–486.
615 https://doi.org/10.1016/j.tplants.2012.04.001.
616 Berendsen, R. L., Vismans, G., Yu, K., Song, Y., de Jonge, R., Burgman, W. P., Burmølle, M.,
617 Herschend, J., Bakker, P. A. H. M., and Pieterse, C. M. J. 2018. Disease-induced assemblage
618 of a plant-beneficial bacterial consortium. **ISME J.** 12:1496–1507.
619 https://doi.org/10.1038/s41396-018-0093-1.
620 Blin, K., Shaw, S., Augustijn, H. E., Reitz, Z. L., Biermann, F., Alanjary, M., Fetter, A., Terlouw,
621 B. R., Metcalf, W. W., Helfrich, E. J. N., van Wezel, G. P., Medema, M. H., and Weber, T.
622 2023. antiSMASH 7.0: new and improved predictions for detection, regulation, chemical
623 structures and visualization. **Nucleic Acids Res.** 51:W46–W50.
624 https://doi.org/10.1093/nar/gkad344.
625 Bloem, E., Haneklaus, S., and Schnug, E. 2015. Milestones in plant sulfur research on sulfur-
626 induced-resistance (SIR) in Europe. **Front. Plant Sci.** 5.
627 https://doi.org/10.3389/fpls.2014.00779.
628 Boccacci, P., and Botta, R. 2009. Investigating the origin of hazelnut (*Corylus avellana* L.)
629 cultivars using chloroplast microsatellites. **Genet. Resour. Crop Evol.** 56:851–859.
630 https://doi.org/10.1007/s10722-009-9406-6.
631 Bolger, A. M., Lohse, M., and Usadel, B. 2014. Trimmomatic: a flexible trimmer for Illumina
632 sequence data. **Bioinformatics** 30:2114–2120.
633 https://doi.org/10.1093/bioinformatics/btu170.
634 Bonito, G., Reynolds, H., Robeson II, M. S., Nelson, J., Hodkinson, B. P., Tuskan, G., Schadt, C.

635 W., and Vilgalys, R. 2014. Plant host and soil origin influence fungal and bacterial
636 assemblages in the roots of woody plants. **Mol. Ecol.** 23:3356–3370.
637 https://doi.org/10.1111/mec.12821.
638 Bouffaud, M., Poirier, M., Muller, D., and Moënne-Loccoz, Y. 2014. Root microbiome relates to
639 plant host evolution in maize and other Poaceae. **Environ. Microbiol.** 16:2804–2814.
640 https://doi.org/10.1111/1462-2920.12442.
641 Bushnell, B. 2014. BBMap: a fast, accurate, splice-aware aligner.
642 https://www.osti.gov/biblio/1241166.
643 Capik, J. M., Muehlbauer, M., Novy, A., Honig, J. A., & Molnar, T. J. 2013. Eastern Filbert Blight-
644 resistant hazelnuts from Russia, Ukraine, and Poland. **HortScience** 48:466–
645 473. https://doi.org/10.21273/HORTSCI.48.4.466.
646 Cavaletti, L., Monciardini, P., Schumann, P., Rohde, M., Bamonte, R., Busti, E., Sosio, M., and
647 Donadio, S. 2006. *Actinospica robiniae* gen. nov., sp. nov. and *Actinospica acidiphila* sp.
648 nov.: proposal for *Actinospicaceae* fam. nov. and *Catenulisporinae* subord. nov. in the order
649 *Actinomycetales*. **Int. J. Syst. Evol. Microbiol.** 56:1747–1753.
650 https://doi.org/10.1099/ijs.0.63859-0.
651 Chaumeil, P.-A., Mussig, A. J., Hugenholtz, P., and Parks, D. H. 2020. GTDB-Tk: a toolkit to
652 classify genomes with the Genome Taxonomy Database. **Bioinformatics** 36:1925–1927.
653 https://doi.org/10.1093/bioinformatics/btz848.
654 Cheng, Y., Sun, S., Lou, H., Dong, Y., He, H., Mei, Q., and Liu, J. 2024. The ectomycorrhizal
655 fungus *Scleroderma bovista* improves growth of hazelnut seedlings and plays a role in auxin
656 signaling and transport. **Front. Microbiol**. 15. https://doi.org/10.3389/fmicb.2024.1431120.
657 Demain, A. L., and Fang, A. 2000. The natural functions of secondary metabolites. **Adv. Biochem.**

658 **Eng. Biotechnol.** 69:1–39. https://doi.org/10.1007/3-540-44964-7_1.

659 Derikvand, F., Bazgir, E., El Jarroudi, M., Darvishnia, M., Mirzaei Najafgholi, H., Laasli, S.-E.,
660 and Lahlali, R. 2023. Unleashing the potential of bacterial isolates from apple tree
661 rhizosphere for biocontrol of *Monilinia laxa*: a promising approach for combatting brown
662 rot disease. **J. Fungi** 9:828. https://doi.org/10.3390/jof9080828.

663 Dinno, A. 2024. **dunn.test: dunn's test of multiple comparisons using rank sums**.
664 https://CRAN.R-project.org/package=dunn.test.

665 Dlamini, S. P., Akanmu, A. O., and Babalola, O. O. 2022. Rhizospheric microorganisms: the
666 gateway to a sustainable plant health. **Front. Sustain. Food Syst.** 6:925802.
667 https://doi.org/10.3389/fsufs.2022.925802.

668 Dong, F., Wang, Y., and Tang, M. 2021. Effects of *Laccaria bicolor* on gene expression of *Populus*
669 *trichocarpa* root under poplar canker stress**. J. Fungi** 7:1024.
670 https://doi.org/10.3390/jof7121024.

671 Dordas, C. 2008. Role of nutrients in controlling plant diseases in sustainable agriculture. A review.
672 **Agron. Sustain. Dev.** 28:33–46. https://doi.org/10.1051/agro:2007051.

673 Dotaniya, M. L., and Meena, V. D. 2015. Rhizosphere effect on nutrient availability in soil and its
674 uptake by plants: a review. **Proc. Natl. Acad. Sci. India Sect. B Biol. Sci.** 85:1–12.
675 https://doi.org/10.1007/s40011-013-0297-0.

676 Ezrari, S., Mhidra, O., Radouane, N., Tahiri, A., Polizzi, G., Lazraq, A., and Lahlali, R. 2021.
677 Potential role of rhizobacteria isolated from citrus rhizosphere for biological control of citrus
678 dry root rot. **Plants Basel Switz.** 10:872. https://doi.org/10.3390/plants10050872.

679 Fancy, N. N., Bahlmann, A.-K., and Loake, G. J. 2017. Nitric oxide function in plant abiotic stress.
680 **Plant Cell Environ.** 40:462–472. https://doi.org/10.1111/pce.12707.

681 Fitzpatrick, C. R., Copeland, J., Wang, P. W., Guttman, D. S., Kotanen, P. M., and Johnson, M. T.
682 J. 2018. Assembly and ecological function of the root microbiome across angiosperm plant
683 species. **Proc. Natl. Acad. Sci.** 115:E1157–E1165.
684 https://doi.org/10.1073/pnas.1717617115.
685 Food and Agricultural Organization of the United Nations. 2021. **FAOSTAT**.
686 https://www.fao.org/faostat/en/#data/QCL [Accessed 15 Oct. 2024]
687 Gómez Expósito, R., Postma, J., Raaijmakers, J. M., and De Bruijn, I. 2015. Diversity and activity
688 of *Lysobacter* species from disease suppressive soils. **Front. Microbiol.** 6:1243.
689 https://doi.org/10.3389/fmicb.2015.01243.
690 Gupta, R., Anand, G., Gaur, R., and Yadav, D. 2021. Plant–microbiome interactions for sustainable
691 agriculture: a review. **Physiol. Mol. Biol. Plants** 27:165–179.
692 https://doi.org/10.1007/s12298-021-00927-1.
693 Hakim, S., Naqqash, T., Nawaz, M. S., Laraib, I., Siddique, M. J., Zia, R., Mirza, M. S., and Imran,
694 A. 2021. Rhizosphere engineering with plant growth-promoting microorganisms for
695 agriculture and ecological sustainability. **Front. Sustain. Food Syst.** 5:617157.
696 https://doi.org/10.3389/fsufs.2021.617157.
697 Hancock, J. T. 2020. Nitric oxide signaling in plants. **Plants** 9:1550.
698 https://doi.org/10.3390/plants9111550.
699 Hassani, M. A., Durán, P., and Hacquard, S. 2018. Microbial interactions within the plant
700 holobiont. **Microbiome** 6:58. https://doi.org/10.1186/s40168-018-0445-0.
701 Hayward, A. C., Fegan, N., Fegan, M., and Stirling, G. R. 2010. *Stenotrophomonas* and
702 *Lysobacter*: ubiquitous plant-associated gamma-proteobacteria of developing significance in
703 applied microbiology. **J. Appl. Microbiol.** 108:756–770. https://doi.org/10.1111/j.1365-

704 2672.2009.04471.x.

705 Helmstetter, A. J., Oztolan-Erol, N., Lucas, S. J., and Buggs, R. J. A. 2020. Genetic diversity and
706 domestication of hazelnut (*Corylus avellana* L.) in Turkey. **Plants, People, Planet** 2:326–
707 339. https://doi.org/10.1002/ppp3.10078.

708 Ho, C. H., and Tsay, Y. F. 2010. Nitrate, ammonium, and potassium sensing and signaling. **Curr.**
709 **Opin. Plant Biol.** 13:604–610. https://doi.org/10.1016/j.pbi.2010.08.005.

710 Hyatt, D., Chen, G.-L., LoCascio, P. F., Land, M. L., Larimer, F. W., and Hauser, L. J. 2010.
711 Prodigal: prokaryotic gene recognition and translation initiation site identification. **BMC**
712 **Bioinformatics** 11:119. https://doi.org/10.1186/1471-2105-11-119.

713 Jacobs, D. C., Revord, R. S., Capik, J. M., Mehlenbacher, S. A., and Molnar, T. J. 2024a. Variable
714 response of eastern filbert blight resistance sources in New Jersey. **Front. Plant Sci.** 15.
715 https://doi.org/10.3389/fpls.2024.1419265.

716 Jacobs, D. C., Revord, R. S., Capik, J. M., and Molnar, T. J. 2024b. Eastern filbert blight
717 resistant *Corylus avellana* identified from 20 years of germplasm introduction and
718 evaluation at Rutgers University, New Jersey, USA. **Front. Plant Sci.** 15.
719 https://doi.org/10.3389/fpls.2024.1502392.

720 Jeger, M., Bragard, C., Caffier, D., Candresse, T., Chatzivassiliou, E., Dehnen-Schmutz, K.,
721 Gilioli, G., Grégoire, J., Jaques Miret, J. A., MacLeod, A., Navajas Navarro, M., Niere, B.,
722 Parnell, S., Potting, R., Rafoss, T., Rossi, V., Urek, G., Van Bruggen, A., Van der Werf, W.,
723 West, J., Winter, S., Boberg, J., Gonthier, P., and Pautasso, M. 2018. Pest categorization of
724 *Anisogramma anomala*. **EFSA J.** 16:e05184. https://doi.org/10.2903/j.efsa.2018.5184.

725 Jiang, H., Xu, X., Fang, Y., Ogunyemi, S. O., Ahmed, T., Li, X., Yang, Y., Yan, C., Chen, J., and
726 Li, B. 2023. Metabarcoding reveals response of rice rhizosphere bacterial community to rice

727 bacterial leaf blight. **Microbiol. Res.** 270:127344.
728 https://doi.org/10.1016/j.micres.2023.127344.
729 Jones, D. L., and Hinsinger, P. 2008. The rhizosphere: complex by design. **Plant Soil** 312:1–6.
730 https://doi.org/10.1007/s11104-008-9774-2.
731 Kalyaanamoorthy, S., Minh, B. Q., Wong, T. K. F., von Haeseler, A., and Jermiin, L. S. 2017.
732 ModelFinder: fast model selection for accurate phylogenetic estimates. **Nat. Methods**
733 14:587–589. https://doi.org/10.1038/nmeth.4285.
734 Kang, D. D., Li, F., Kirton, E., Thomas, A., Egan, R., An, H., and Wang, Z. 2019. MetaBAT 2: an
735 adaptive binning algorithm for robust and efficient genome reconstruction from metagenome
736 assemblies. **PeerJ.** 7:e7359. https://doi.org/10.7717/peerj.7359.
737 Kassambara, A. 2025. **ggpubr: 'ggplot2' based publication ready plots**. https://CRAN.R-
738 project.org/package=ggpubr.
739 Kebert, M., Kostić, S., Zlatković, M., Stojnic, S., Čapelja, E., Zorić, M., Kiprovski, B., Budakov,
740 D., and Orlović, S. 2022. Ectomycorrhizal fungi modulate biochemical response against
741 powdery mildew disease in *Quercus robur* L. **Forests** 13:1491.
742 https://doi.org/10.3390/f13091491.
743 Khan, M., Al Azawi, T. N. I., Pande, A., Mun, B.-G., Lee, D.-S., Hussain, A., Lee, B.-H., and Yun,
744 B.-W. 2021. The role of nitric oxide-induced ATILL6 in growth and disease resistance in
745 *Arabidopsis thaliana*. **Front. Plant Sci.** 12. https://doi.org/10.3389/fpls.2021.685156.
746 Kilic-Ekici, O., and Yuen, G. Y. 2003. Induced resistance as a mechanism of biological control by
747 *Lysobacter enzymogenes* strain C3**.** **Phytopathology** 93:1103–1110.
748 https://doi.org/10.1094/PHYTO.2003.93.9.1103.
749 Künstler, A., Gullner, G., Ádám, A. L., Kolozsváriné Nagy, J., and Király, L. 2020. The versatile

750 roles of sulfur-containing biomolecules in plant defense—a road to disease resistance. **Plants**
751 9:1705. https://doi.org/10.3390/plants9121705.
752 Kurtz, S., Phillippy, A., Delcher, A. L., Smoot, M., Shumway, M., Antonescu, C., and Salzberg, S.
753 L. 2004. Versatile and open software for comparing large genomes. **Genome Biol.** 5:R12.
754 https://doi.org/10.1186/gb-2004-5-2-r12.
755 Kusuma, A. B., Putra, K. E., Vanggy, L. R., Loh, J., Nouioui, I., and Goodfellow, M. 2022.
756 *Actinospica acidithermotolerans* sp. nov., a novel actinomycete isolated from sediment from
757 an Indonesian hot spring. **Arch. Microbiol.** 204:518. https://doi.org/10.1007/s00203-022-
758 03058-7.
759 Lahti, L., and Shetty, S. 2019. **microbiome R package**. http://microbiome.github.io
760 Langmead, B., and Salzberg, S. L. 2012. Fast gapped-read alignment with Bowtie 2. **Nat. Methods**
761 9:357–359. https://doi.org/10.1038/nmeth.1923.
762 Lee, S., Yap, M., Behringer, G., Hung, R., and Bennett, J. W. 2016. Volatile organic compounds
763 emitted by *Trichoderma* species mediate plant growth. **Fungal Biol. Biotechnol.** 3:7.
764 https://doi.org/10.1186/s40694-016-0025-7.
765 Lei, S., Xu, X., Cheng, Z., Xiong, J., Ma, R., Zhang, L., Yang, X., Zhu, Y., Zhang, B., and Tian, B.
766 2019. Analysis of the community composition and bacterial diversity of the rhizosphere
767 microbiome across different plant taxa. **MicrobiologyOpen** 8:e00762.
768 https://doi.org/10.1002/mbo3.762.
769 Letunic, I., and Bork, P. 2024. Interactive Tree of Life (iTOL) v6: recent updates to the
770 phylogenetic tree display and annotation tool. **Nucleic Acids Res.** 52:W78–W82.
771 https://doi.org/10.1093/nar/gkae268.
772 Li, D., Liu, C. M., Luo, R., Sadakane, K., and Lam, T.-W. 2015. MEGAHIT: an ultra-fast single-

773 node solution for large and complex metagenomics assembly via succinct de Bruijn graph.
774 **Bioinformatics** 31:1674–1676. https://doi.org/10.1093/bioinformatics/btv033.
775 Li, H. 2018. Minimap2: pairwise alignment for nucleotide sequences. **Bioinformatics** 34:3094–
776 3100. https://doi.org/10.1093/bioinformatics/bty191.
777 Li, H., Handsaker, B., Wysoker, A., Fennell, T., Ruan, J., Homer, N., Marth, G., Abecasis, G.,
778 Durbin, R., and 1000 Genome Project Data Processing Subgroup. 2009. The sequence
779 alignment/map format and SAMtools. **Bioinformatics** 25:2078–2079.
780 https://doi.org/10.1093/bioinformatics/btp352.
781 Li, Z., Li, J., Liu, G., Li, Y., Wu, X., Liang, J., Wang, Z., Chen, Q., and Peng, F. 2025. Isolation,
782 characterization and growth-promoting properties of phosphate-solubilizing bacteria (PSBs)
783 derived from peach tree rhizosphere. **Microorganisms** 13:718.
784 https://doi.org/10.3390/microorganisms13040718.
785 Lin, H., and Peddada, S. D. 2024. Multigroup analysis of compositions of microbiomes with
786 covariate adjustments and repeated measures. **Nat. Methods** 21:83–91.
787 https://doi.org/10.1038/s41592-023-02092-7.
788 Liu, F., Hewezi, T., Lebeis, S. L., Pantalone, V., Grewal, P. S., and Staton, M. E. 2019. Soil
789 indigenous microbiome and plant genotypes cooperatively modify soybean rhizosphere
790 microbiome assembly. **BMC Microbiol.** 19:201. https://doi.org/10.1186/s12866-019-1572-
791 x.
792 Liu, H., Li, J., Carvalhais, L. C., Percy, C. D., Prakash Verma, J., Schenk, P. M., and Singh, B. K.
793 2021. Evidence for the plant recruitment of beneficial microbes to suppress soil-borne
794 pathogens. **New Phytol.** 229:2873–2885. https://doi.org/10.1111/nph.17057.
795 Liu, L., Ma, L., Zhu, M., Liu, B., Liu, X., and Shi, Y. 2023b. Rhizosphere microbial community

796 assembly and association networks strongly differ based on vegetation type at a local
797 environment scale. **Front. Microbiol.** 14:1129471.
798 https://doi.org/10.3389/fmicb.2023.1129471.
799 Liu, S., Tao, C., Zhang, L., Wang, Z., Xiong, W., Xiang, D., Sheng, O., Wang, J., Li, R., Shen, Z.,
800 Li, C., Shen, Q., and Kowalchuk, G. A. 2023a. Plant pathogen resistance is mediated by
801 recruitment of specific rhizosphere fungi. **ISME J.** 17:931–942.
802 https://doi.org/10.1038/s41396-023-01406-z.
803 Lopes, A. C. de A., Mendes, L. W., Brito, K. A. da S. B., da Silva, J. L., Rocha, S. M. B., Antunes,
804 J. E. L., Oliveira, L. M. de S., Melo, V. M. M., Oliveira, F. A. S., Pereira, A. P. de A., Costa,
805 G. do N., da Silva, V. B., Gomes, R. L. F., de Alcantara Neto, F., and Araujo, A. S. F. 2023.
806 Rhizospheric microbial community in plant species from the *Phaseolus* genus. **Appl. Soil**
807 **Ecol.** 182:104731. https://doi.org/10.1016/j.apsoil.2022.104731.
808 Lotfi, N., Soleimani, A., Çakmakçı, R., Vahdati, K., and Mohammadi, P. 2022. Characterization of
809 plant growth-promoting rhizobacteria (PGPR) in Persian walnut associated with drought
810 stress tolerance. **Sci. Rep.** 12:12725. https://doi.org/10.1038/s41598-022-16852-6.
811 Lu, J., Breitwieser, F., Thielen, P., and Salzberg, S. 2017. Bracken: estimating species abundance
812 in metagenomics data. **PeerJ Comput. Sci.** 3:e104. https://doi.org/10.7717/peerj-cs.104.
813 Luciani, E., Palliotti, A., Tombesi, S., Gardi, T., Micheli, M., Berrios, J. G., Zadra, C., and Farinelli,
814 D. 2019. Mitigation of multiple summer stresses on hazelnut (*Corylus avellana* L.): effects
815 of the new arbuscular mycorrhiza *Glomus iranicum tenuihypharum* sp. *nova*. **Sci. Hortic.**
816 257:108659. https://doi.org/10.1016/j.scienta.2019.108659.
817 Luo, L., Zhang, J., Ye, C., Li, S., Duan, S., Wang, Z., Huang, H., Liu, Y., Deng, W., Mei, X.,
818 He, X., Yang, M., Zhu, S. 2022. Foliar pathogen infection manipulates soil health through

819 root exudate-modified rhizosphere microbiome. **Microbiol Spectr** 10:e02418-22.
820 https://doi.org/10.1128/spectrum.02418-22
821 Ma, W., Yang, Z., Liang, L., Ma, Q., Wang, G., and Zhao, T. 2021. Characteristics of the fungal
822 communities and co-occurrence networks in hazelnut tree root endospheres and rhizosphere
823 soil. **Front. Plant Sci.** 12. https://doi.org/10.3389/fpls.2021.749871.
824 Majer, H. M., Ehrlich, R. L., Ahmed, A., Earl, J. P., Ehrlich, G. D., and Beld, J. 2021. Whole
825 genome sequencing of *Streptomyces actuosus* ISP-5337, *Streptomyces sioyaensis* B-5408,
826 and *Actinospica acidiphila* B-2296 reveals secondary metabolomes with antibiotic potential.
827 **Biotechnol. Rep.** 29:e00596. https://doi.org/10.1016/j.btre.2021.e00596.
828 Martinez Arbizu, P. 2017. **pairwiseAdonis: pairwise multilevel comparison using adonis**.
829 https://github.com/pmartinezarbizu/pairwiseAdonis.
830 Matsen, F. A., Kodner, R. B., and Armbrust, E. V. 2010. pplacer: linear time maximum-likelihood
831 and Bayesian phylogenetic placement of sequences onto a fixed reference tree. **BMC**
832 **Bioinformatics** 11:538. https://doi.org/10.1186/1471-2105-11-538.
833 McMurdie, P. J., and Holmes, S. 2013. phyloseq: an R package for reproducible interactive
834 analysis and graphics of microbiome census data. **PLOS ONE** 8:e61217.
835 https://doi.org/10.1371/journal.pone.0061217.
836 Minh, B. Q., Schmidt, H. A., Chernomor, O., Schrempf, D., Woodhams, M. D., von Haeseler, A.,
837 and Lanfear, R. 2020. IQ-TREE 2: new models and efficient methods for phylogenetic
838 inference in the genomic era. **Mol. Biol. Evol.** 37:1530–1534.
839 https://doi.org/10.1093/molbev/msaa015.
840 Molnar, T. J. 2011. Corylus. Pages 15–48 in: ***Wild Crop Relatives: Genomic and Breeding***
841 ***Resources: Forest Trees***. C. Kole, ed. Springer, Heidelberg, Germany.

842 https://doi.org/10.1007/978-3-642-21250-5_2.

843 Mur, L. A. J., Simpson, C., Kumari, A., Gupta, A. K., and Gupta, K. J. 2017. Moving nitrogen to
844 the centre of plant defence against pathogens. **Ann. Bot.** 119:703–709.
845 https://doi.org/10.1093/aob/mcw179.

846 Nasir, N. N. M., Ho, C.-L., Lamasudin, D. U., and Saidi, N. B. 2020. Nitric oxide improves
847 tolerance to *Fusarium oxysporum* f. sp. cubense tropical race 4 in banana. **Physiol. Mol.**
848 **Plant Pathol.** 111:101503. https://doi.org/10.1016/j.pmpp.2020.101503.

849 Navarro-Muñoz, J. C., Selem-Mojica, N., Mullowney, M. W., Kautsar, S. A., Tryon, J. H.,
850 Parkinson, E. I., De Los Santos, E. L. C., Yeong, M., Cruz-Morales, P., Abubucker, S.,
851 Roeters, A., Lokhorst, W., Fernandez-Guerra, A., Cappelini, L. T. D., Goering, A. W.,
852 Thomson, R. J., Metcalf, W. W., Kelleher, N. L., Barona-Gomez, F., and Medema, M. H.
853 2020. A computational framework to explore large-scale biosynthetic diversity. **Nat. Chem.**
854 **Biol.** 16:60–68. https://doi.org/10.1038/s41589-019-0400-9.

855 Nissen, J. N., Johansen, J., Allesøe, R. L., Sønderby, C. K., Armenteros, J. J. A., Grønbech, C. H.,
856 Jensen, L. J., Nielsen, H. B., Petersen, T. N., Winther, O., and Rasmussen, S. 2021. Improved
857 metagenome binning and assembly using deep variational autoencoders. **Nat. Biotechnol.**
858 39:555–560. https://doi.org/10.1038/s41587-020-00777-4.

859 Oksanen, J., Simpson, G. L., Blanchet, F. G., Kindt, R., Legendre, P., Minchin, P. R., O'Hara, R.
860 B., Solymos, P., Stevens, M. H. H., Szoecs, E., Wagner, H., Barbour, M., Bedward, M.,
861 Bolker, B., Borcard, D., Carvalho, G., Chirico, M., De Caceres, M., Durand, S.,
862 Evangelista, H. B. A., FitzJohn, R., Friendly, M., Furneaux, B., Hannigan, G., Hill, M.
863 O., Lahti, L., McGlinn, D., Ouellette, M.-H., Ribeiro Cunha, E., Smith, T., Stier, A., Ter
864 Braak, C. J. F., and Weedon, J. 2024. **vegan: Community Ecology Package**.

865 https://CRAN.R-project.org/package=vegan
866 Olm, M. R., Brown, C. T., Brooks, B., and Banfield, J. F. 2017. dRep: a tool for fast and accurate
867 genomic comparisons that enables improved genome recovery from metagenomes through
868 de-replication. **ISME J.** 11:2864–2868. https://doi.org/10.1038/ismej.2017.126.
869 Ondov, B. D., Bergman, N. H., and Phillippy, A. M. 2011. Interactive metagenomic visualization
870 in a web browser. **BMC Bioinformatics** 12:385. https://doi.org/10.1186/1471-2105-12-385.
871 Ondov, B. D., Treangen, T. J., Melsted, P., Mallonee, A. B., Bergman, N. H., Koren, S., and
872 Phillippy, A. M. 2016. Mash: fast genome and metagenome distance estimation using
873 MinHash. **Genome Biol.** 17:132. https://doi.org/10.1186/s13059-016-0997-x.
874 Orozco-Mosqueda, Ma. D. C., Fadiji, A. E., Babalola, O. O., Glick, B. R., and Santoyo, G. 2022.
875 Rhizobiome engineering: unveiling complex rhizosphere interactions to enhance plant
876 growth and health. **Microbiol. Res.** 263:127137.
877 https://doi.org/10.1016/j.micres.2022.127137.
878 Pan, S., Zhao, X.-M., and Coelho, L. P. 2023. SemiBin2: self-supervised contrastive learning leads
879 to better MAGs for short- and long-read sequencing. **Bioinformatics** 39:i21–i29.
880 https://doi.org/10.1093/bioinformatics/btad209.
881 Pantigoso, H. A., Newberger, D., and Vivanco, J. M. 2022. The rhizosphere microbiome: plant–
882 microbial interactions for resource acquisition. **J. Appl. Microbiol.** 133:2864–2876.
883 https://doi.org/10.1111/jam.15686.
884 Parks, D. H., Imelfort, M., Skennerton, C. T., Hugenholtz, P., and Tyson, G. W. 2015. CheckM:
885 assessing the quality of microbial genomes recovered from isolates, single cells, and
886 metagenomes. **Genome Res.** 25:1043–1055. https://doi.org/10.1101/gr.186072.114.
887 Pedersen, T. L. 2019. **patchwork: The Composer of Plots**. http://CRAN.R-

project.org/package=patchwork

Peiffer, J. A., Spor, A., Koren, O., Jin, Z., Tringe, S. G., Dangl, J. L., Buckler, E. S., and Ley, R. E. 2013. Diversity and heritability of the maize rhizosphere microbiome under field conditions. **Proc. Natl. Acad. Sci.** 110:6548–6553. https://doi.org/10.1073/pnas.1302837110.

Pinkerton, J. N. 1995. Infection of European hazelnut by *Anisogramma anomala*: ascospore adhesion, mode of penetration of immature shoots, and host response. **Phytopathology** 85:1260. https://doi.org/10.1094/Phyto-85-1260.

Poomthongdee, N., Duangmal, K., and Pathom-aree, W. 2015. Acidophilic actinomycetes from rhizosphere soil: diversity and properties beneficial to plants. **J. Antibiot.** 68:106–114. https://doi.org/10.1038/ja.2014.117.

Puopolo, G., Giovannini, O., and Pertot, I. 2014. *Lysobacter capsici* AZ78 can be combined with copper to effectively control *Plasmopara viticola* on grapevine. **Microbiol. Res.** 169:633–642. https://doi.org/10.1016/j.micres.2013.09.013.

Qi, G., Ma, G., Chen, S., Lin, C., and Zhao, X. 2019. Microbial network and soil properties are changed in bacterial wilt-susceptible soil. **Appl. Environ. Microbiol.** 85:e00162-19. https://doi.org/10.1128/AEM.00162-19.

Qiao, H., Gao, D., and Yuan, T. 2023. Differences in rhizosphere soil fungal communities of wild and cultivated *Paeonia ludlowii* species. **Front. Plant Sci.** 14. https://doi.org/10.3389/fpls.2023.1194598.

Ranjan, A., Rajput, V. D., Prazdnova, E. V., Gurnani, M., Bhardwaj, P., Sharma, S., Sushkova, S., Mandzhieva, S. S., Minkina, T., Sudan, J., Zargar, S. M., Chauhan, A., and Jindal, T. 2023. Nature's antimicrobial arsenal: non-ribosomal peptides from PGPB for plant pathogen biocontrol. **Fermentation** 9:597. https://doi.org/10.3390/fermentation9070597.

911 R Core Team. 2025. The R Project for Statistical Computing. https://www.R-project.org/

912 Revord, R. S., Lovell, S. T., Capik, J. M., Mehlenbacher, S. A., and Molnar, T. J. 2020. Eastern
913 filbert blight resistance in American and interspecific hybrid hazelnuts. **J. Am. Soc. Hortic.**
914 **Sci.** 145:162–173. https://doi.org/10.21273/JASHS04732-19.

915 Rodriguez-Mena, S., Camacho, M., de los Santos, B., Miranda, L., and Camacho-Sanchez, M.
916 2022. Microbiota modulation in blueberry rhizosphere by biocontrol bacteria. **Microbiol.**
917 **Res.** 13:809–824. https://doi.org/10.3390/microbiolres13040057.

918 Rostamikia, Y., Tabari Kouchaksaraei, M., Asgharzadeh, A., and Rahmani, A. 2017. Effect of
919 growth promoting rhizobacteria on growth and nutrient elements of common hazelnut
920 (*Corylus avellana* L.) seedlings in Ardabil Fandoqlou nursery. **Iran. J. For. Poplar Res.**
921 25:126–116. https://doi.org/10.22092/ijfpr.2017.109781.

922 Ruparelia, J., Rabari, A., Mitra, D., Panneerselvam, P., Das-mohapatra, P. K., and Jha, C. K. 2022.
923 Efficient applications of bacterial secondary metabolites for management of biotic stress in
924 plants. **Plant Stress** 6:100125. https://doi.org/10.1016/j.stress.2022.100125.

925 Santoyo, G. 2022. How plants recruit their microbiome? New insights into beneficial interactions.
926 **J. Adv. Res.** 40:45–58. https://doi.org/10.1016/j.jare.2021.11.020.

927 Shaffer, M., Borton, M. A., McGivern, B. B., Zayed, A. A., La Rosa, S. L., Solden, L. M., Liu, P.,
928 Narrowe, A. B., Rodríguez-Ramos, J., Bolduc, B., Gazitúa, M. C., Daly, R. A., Smith, G. J.,
929 Vik, D. R., Pope, P. B., Sullivan, M. B., Roux, S., and Wrighton, K. C. 2020. DRAM for
930 distilling microbial metabolism to automate the curation of microbiome function. **Nucleic**
931 **Acids Res.** 48:8883–8900. https://doi.org/10.1093/nar/gkaa621.

932 Sharrar, A. M., Crits-Christoph, A., Méheust, R., Diamond, S., Starr, E. P., and Banfield, J. F. 2020.
933 Bacterial secondary metabolite biosynthetic potential in soil varies with phylum, depth, and

934 vegetation type. **mBio** 11:e00416-20. https://doi.org/10.1128/mBio.00416-20.

935 Sieber, C. M. K., Probst, A. J., Sharrar, A., Thomas, B. C., Hess, M., Tringe, S. G., and Banfield,
936 J. F. 2018. Recovery of genomes from metagenomes via a dereplication, aggregation and
937 scoring strategy. **Nat. Microbiol.** 3:836–843. https://doi.org/10.1038/s41564-018-0171-1.

938 Sillo, F., Brunetti, C., Marroni, F., Vita, F., dos Santos Nascimento, L. B., Vizzini, A., Mello, A.,
939 and Balestrini, R. 2022. Systemic effects of *Tuber melanosporum* inoculation in two *Corylus*
940 *avellana* genotypes. **Tree Physiol.** 42:1463–1480. https://doi.org/10.1093/treephys/tpac012.

941 Sood, M., Kapoor, D., Kumar, V., Sheteiwy, M. S., Ramakrishnan, M., Landi, M., Araniti, F., and
942 Sharma, A. 2020. Trichoderma: The "secrets" of a multitalented biocontrol agent. **Plants**
943 9:762. https://doi.org/10.3390/plants9060762.

944 Steinegger, M., and Söding, J. 2017. MMseqs2 enables sensitive protein sequence searching for
945 the analysis of massive data sets. **Nat. Biotechnol.** 35:1026–1028.
946 https://doi.org/10.1038/nbt.3988.

947 Sun, C., Zhang, Y., Liu, L., Liu, X., Li, B., Jin, C., and Lin, X. 2021. Molecular functions of nitric
948 oxide and its potential applications in horticultural crops. **Hortic. Res.** 8:1–17.
949 https://doi.org/10.1038/s41438-021-00500-7.

950 Sun, Y., Wang, M., Mur, L. A. J., Shen, Q., and Guo, S. 2020. Unravelling the roles of nitrogen
951 nutrition in plant disease defenses. **Int. J. Mol. Sci.** 21:572.
952 https://doi.org/10.3390/ijms21020572.

953 Thepbandit, W., and Athinuwat, D. 2024. Rhizosphere microorganisms supply availability of soil
954 nutrients and induce plant defense. **Microorganisms** 12:558.
955 https://doi.org/10.3390/microorganisms12030558.

956 Thompson, M. M., Lagerstedt, H. B., and Mehlenbacher, S. A. 1996. Hazelnuts. Pages 125–184

957 in: **Fruit Breeding, vol. III Nuts.** J. Janick, and N. Moore, eds. John Wiley and Sons Inc,
958 New York, U.S.A.
959 Wang, Y., Yang, Q., Tosa, Y., Nakayashiki, H., and Mayama, S. 2005. Nitric oxide-overproducing
960 transformants of *Pseudomonas fluorescens* with enhanced biocontrol of tomato bacterial
961 wilt. J. **Gen. Plant Pathol.** 71:33–38. https://doi.org/10.1007/s10327-004-0157-0.
962 Wattenburger, C. J., Halverson, L. J., and Hofmockel, K. S. 2019. Agricultural management affects
963 root-associated microbiome recruitment over maize development. **Phytobiomes J.** 3:260–
964 272. https://doi.org/10.1094/PBIOMES-03-19-0016-R.
965 Wickham, H. 2009. **ggplot2: Elegant Graphics for Data Analysis**. Springer, New York, U.S.A.
966 https://doi.org/10.1007/978-0-387-98141-3
967 Wickham, H., François, R., Henry, L., and Müller, K. 2018. **dplyr: A Grammar of Data**
968 **Manipulation**. https://CRAN.Rproject.org/package=dplyr.
969 Wickham, H., Averick, M., Bryan, J., Chang, W., McGowan L. D., François, R., Grolemund, G.,
970 Hayes, A., Henry, L., Hester, J., Kuhn, M., Pedersen, T. L., Miller, E., Bache S. M.,
971 Müller, K., Ooms, J., Robinson, D., Seidel, D. P., Spinu, V., Takahashi, K., Vaughan, D.,
972 Wilke, C., Woo, K., Yutani, H. 2019. Welcome to the tidyverse. **Journal of Open Source**
973 **Software** 4:1686. https://doi.org/10.21105/joss.01686>
974
975 Wood, D. E., Lu, J., and Langmead, B. 2019. Improved metagenomic analysis with Kraken
976 **Genome Biol.** 20:257. https://doi.org/10.1186/s13059-019-1891-0.
977 Wu, Y.-W., Simmons, B. A., and Singer, S. W. 2016. MaxBin 2.0: an automated binning algorithm
978 to recover genomes from multiple metagenomic datasets. **Bioinformatics** 32:605–607.
979 https://doi.org/10.1093/bioinformatics/btv638.

980 Yang, J., Wei, S., Su, D., Zhang, Z., Chen, S., Luo, Z., Shen, X., Lai, Y., Jamil, A., Tong, J., and
981 Cui, X. 2020. Comparison of the rhizosphere soil microbial community structure and
982 diversity between powdery mildew-infected and noninfected strawberry plants in a
983 greenhouse by high-throughput sequencing technology. **Curr. Microbiol.** 77:1724–1736.
984 https://doi.org/10.1007/s00284-020-01948-x.
985 Yu, Y., Gui, Y., Li, Z., Jiang, C., Guo, J., and Niu, D. 2022. Induced systemic resistance for
986 improving plant immunity by beneficial microbes. **Plants** 11:386.
987 https://doi.org/10.3390/plants11030386.
988 Yue, H., Yue, W., Jiao, S., Kim, H., Lee, Y.-H., Wei, G., Song, W., and Shu, D. 2023. Plant
989 domestication shapes rhizosphere microbiome assembly and metabolic functions.
990 **Microbiome** 11:70. https://doi.org/10.1186/s40168-023-01513-1.
991 Zhang, F., Wen, S., Wang, B., Zhang, Z., Liu, F., Ye, T., Wang, K., Hu, H., Yang, X., and Fang, W.
992 2023. Biocontrol potential of *Streptomyces odonnellii* SZF-179 toward *Alternaria alternata*
993 to control pear black spot disease. **Int. J. Mol. Sci.** 24:17515.
994 https://doi.org/10.3390/ijms242417515.
995 Zhang, J., Cook, J., Nearing, J. T., Zhang, J., Raudonis, R., Glick, B. R., Langille, M. G. I., and
996 Cheng, Z. 2021. Harnessing the plant microbiome to promote the growth of agricultural
997 crops. **Microbiol. Res.** 245:126690. https://doi.org/10.1016/j.micres.2020.126690.
998 Zhang, M., Chai, L., Huang, M., Jia, W., Guo, J., and Huang, Y. 2020. Deciphering the archaeal
999 communities in tree rhizosphere of the Qinghai-Tibetan plateau. **BMC Microbiol.** 20:235.
1000 https://doi.org/10.1186/s12866-020-01913-5.
1001

1002 **FIGURE LEGENDS**

1003 **Figure 1. Diversity metrics of the metagenomes.** (**A**, **B**) Alpha diversity values calculated using
1004 the (A) Shannon Diversity Index (Kruskal-Wallis rank sum test, p-value = 0.16) or (B) Simpson
1005 Diversity Index [1-D] (Kruskal-Wallis rank sum test, p-value = 0.06) are shown. Alpha diversity
1006 was calculated based on species level taxonomic classification of assembled contigs (minimum
1007 length of 500 bp). (**C**) A Principal Coordinate Analysis (PCoA) plot based on Bray-Curtis
1008 dissimilarity values is shown (PERMANOVA, p-value < 0.001), with pairwise adonis tests
1009 indicating that the bulk soil was statistically different from the rhizospheres of the native
1010 (p.adjusted = 0.048), susceptible (p.adjusted = 0.047), and resistant (p.adjusted = 0.047) varieties.
1011

1012 **Figure 2. Relative abundance of phyla across the metagenomes.** The abundance of (**A**) bacterial
1013 phyla, (**B**) archaeal phyla, and (**C**) eukaryotic phyla, displayed as a percentage of the total bacteria,
1014 archaea, and eukaryotes, respectively. The rows represent each of the metagenomic samples,
1015 colour coded by group, while the columns represent taxa with an average relative abundance of at
1016 least 1% of bacteria, archaea, or eukaryotes in at least one sample. The legend to the right of the
1017 figure applies to all three panels.
1018

1019 **Figure 3. Relative abundance of genera across the metagenomes.** The abundance of (**A**)
1020 bacterial genera, (**B**) archaeal genera, and (**C**) eukaryotic genera, displayed as a percentage of the
1021 total bacteria, archaea, and eukaryotes, respectively. The rows represent each of the metagenomic
1022 samples, colour coded by group, while the columns represent taxa with an average relative
1023 abundance of at least 1% of bacteria, archaea, or eukaryotes in at least one sample. The size of the
1024 dots corresponds is proportional to the relative abundance of the taxon in a given sample. The

1025 legend below the figure applies to all three panels.

1026

1027 **Figure 4. Global comparison of the metabolic potential of the metagenomes.** A Principal
1028 Coordinate Analysis (PCoA) plot based on Bray-Curtis dissimilarity values calculated from the
1029 KEGG annotations produced for each metagenome using DRAM. While statistically significant
1030 global differences were observed (PERMANOVA, p-value = 0.031), no statistically significant
1031 differences between groups were detected using pairwise adonis tests.

1032

1033 **Figure 5. Putative biosynthetic gene clusters detected in the metagenomes.** (**A**) A heatmap
1034 showing the number of predicted biosynthetic gene clusters summarized by biosynthetic gene
1035 cluster classification. (**B**) A heatmap showing the number of predicted biosynthetic gene clusters
1036 summarized by predicted product. (**A**, **B**) The absence of a box indicates that no genes predicted
1037 to be associated with a particular biosynthetic gene cluster class or product were detected in that
1038 metagenome. The colour of a box represents the number of biosynthetic gene clusters detected as
1039 belonging to a given biosynthetic gene cluster class or product, with deeper red indicating higher
1040 counts.

1041

1042 **Figure 6. Unrooted phylogeny of the bacterial MAGs generated in this study.** An unrooted,
1043 maximum likelihood phylogeny of the 41 high-quality metagenome-assembled genomes (MAGs)
1044 generated in this study, prepared from a concatenated alignment of the bac120 gene set of the
1045 Genome Taxonomy Database. Taxa names and branches are colour coded based on phylum. The
1046 scale represents the mean number of nucleotide substitutions per site. The numbers on the nodes
1047 indicate the SH-aLRT support values (top numbers) and the ultra-fast jackknife values using a

1048 40% resampling rate (bottom numbers), both calculated from 1000 replicates; values are only

1049 shown at nodes where at least one value is below 95.

1050

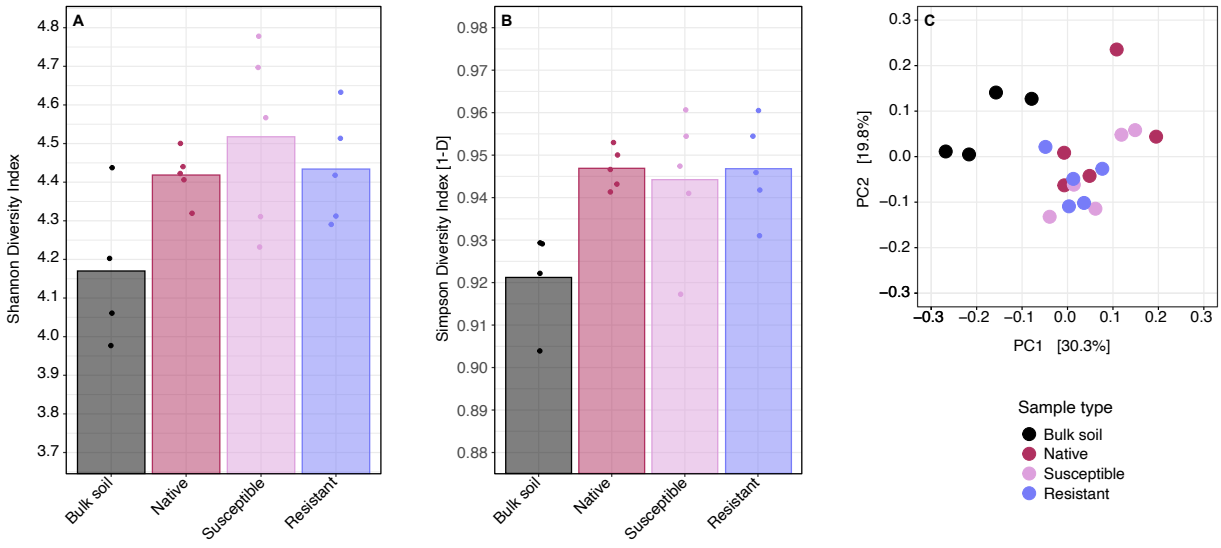

Figure 1. Diversity metrics of the metagenomes. (**A**, **B**) Alpha diversity values calculated using the (A) Shannon Diversity Index (Kruskal-Wallis rank sum test, p-value = 0.16) or (B) Simpson Diversity Index [1-D] (Kruskal-Wallis rank sum test, p-value = 0.06) are shown. Alpha diversity was calculated based on species level taxonomic classification of assembled contigs (minimum length of 500 bp). (**C**) A Principal Coordinate Analysis (PCoA) plot based on Bray-Curtis dissimilarity values is shown (PERMANOVA, p-value < 0.001), with pairwise adonis tests indicating that the bulk soil was statistically different from the rhizospheres of the native (p.adjusted = 0.048), susceptible (p.adjusted = 0.047), and resistant (p.adjusted = 0.047) varieties.

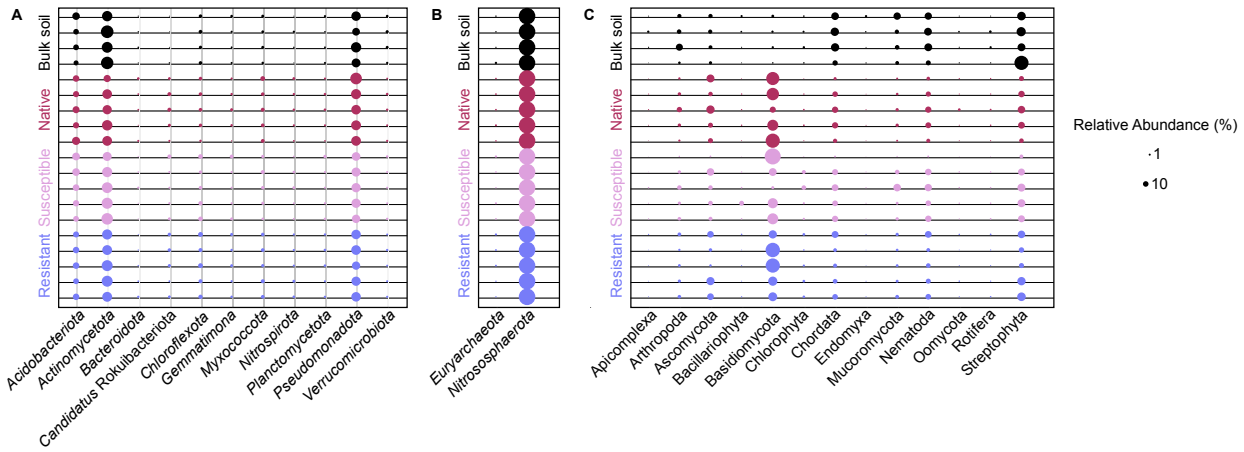

Figure 2. Relative abundance of phyla across the metagenomes. The abundance of (**A**) bacterial phyla, (**B**) archaeal phyla, and (**C**) eukaryotic phyla, displayed as a percentage of the total bacteria, archaea, and eukaryotes, respectively. The rows represent each of the metagenomic samples, colour coded by group, while the columns represent taxa with an average relative abundance of at least 1% of bacteria, archaea, or eukaryotes in at least one sample. The legend to the right of the figure applies to all three panels.

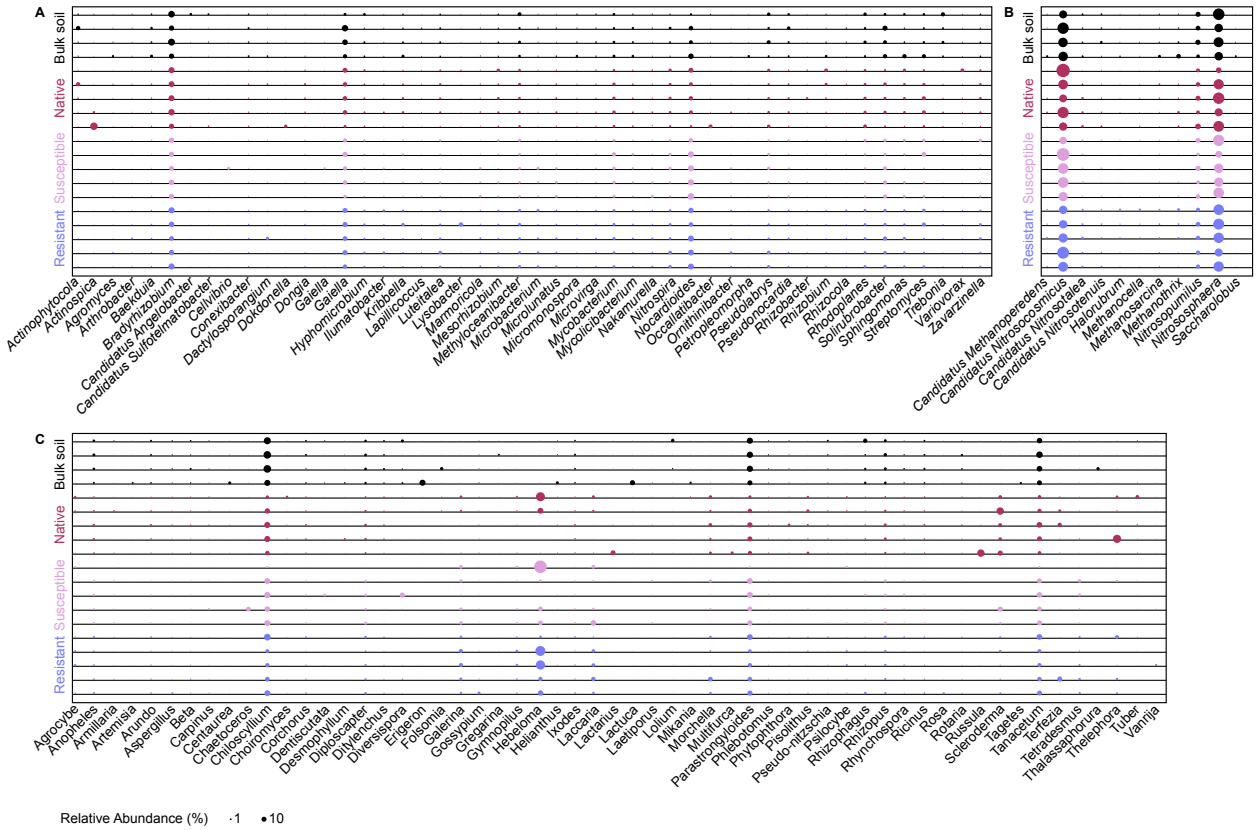

Figure 3. Relative abundance of genera across the metagenomes. The abundance of (**A**) bacterial genera, (**B**) archaeal genera, and (**C**) eukaryotic genera, displayed as a percentage of the total bacteria, archaea, and eukaryotes, respectively. The rows represent each of the metagenomic samples, colour coded by group, while the columns represent taxa with an average relative abundance of at least 1% of bacteria, archaea, or eukaryotes in at least one sample. The size of the dots corresponds is proportional to the relative abundance of the taxon in a given sample. The legend below the figure applies to all three panels.

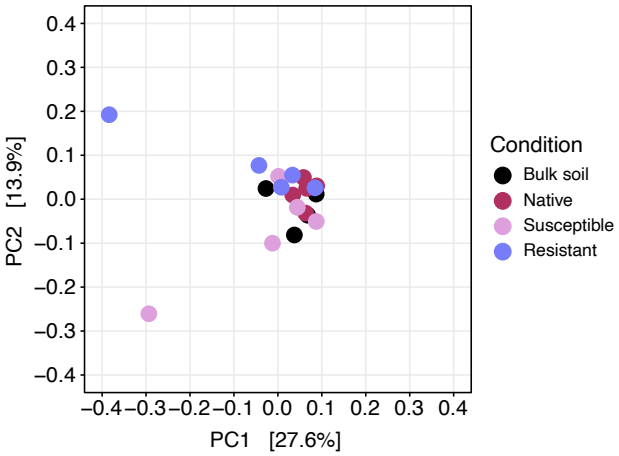

Figure 4. Global comparison of the metabolic potential of the metagenomes. A Principal Coordinate Analysis (PCoA) plot based on Bray-Curtis dissimilarity values calculated from the KEGG annotations produced for each metagenome using DRAM. While statistically significant global differences were observed (PERMANOVA, p-value = 0.031), no statistically significant differences between groups were detected using pairwise adonis tests.

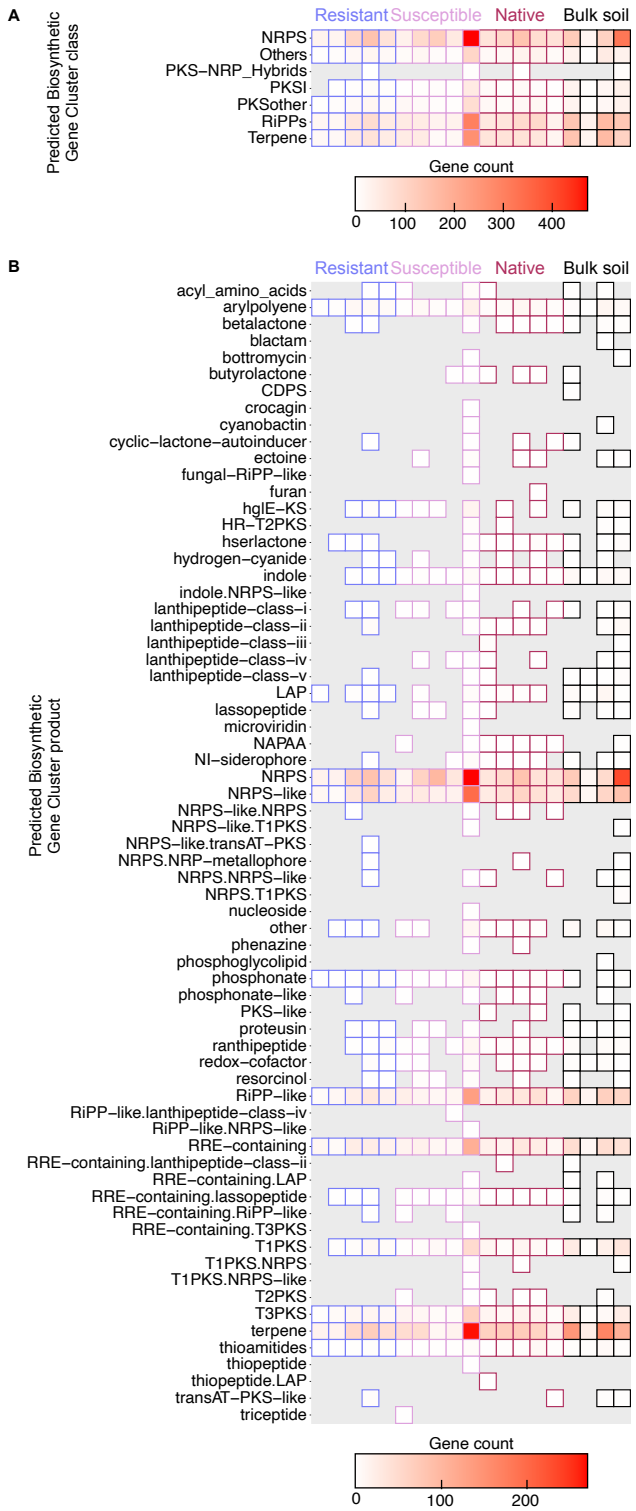

Figure 5. Putative biosynthetic gene clusters detected in the metagenomes. (**A**) A heatmap showing the number of predicted biosynthetic gene clusters summarized by biosynthetic gene cluster classification. (**B**) A heatmap showing the number of predicted biosynthetic gene clusters summarized by predicted product. (**A**, **B**) The absence of a box indicates that no genes predicted to be associated with a particular biosynthetic gene cluster class or product were detected in that metagenome. The colour of a box represents the number of biosynthetic gene clusters detected as belonging to a given biosynthetic gene cluster class or product, with deeper red indicating higher counts.

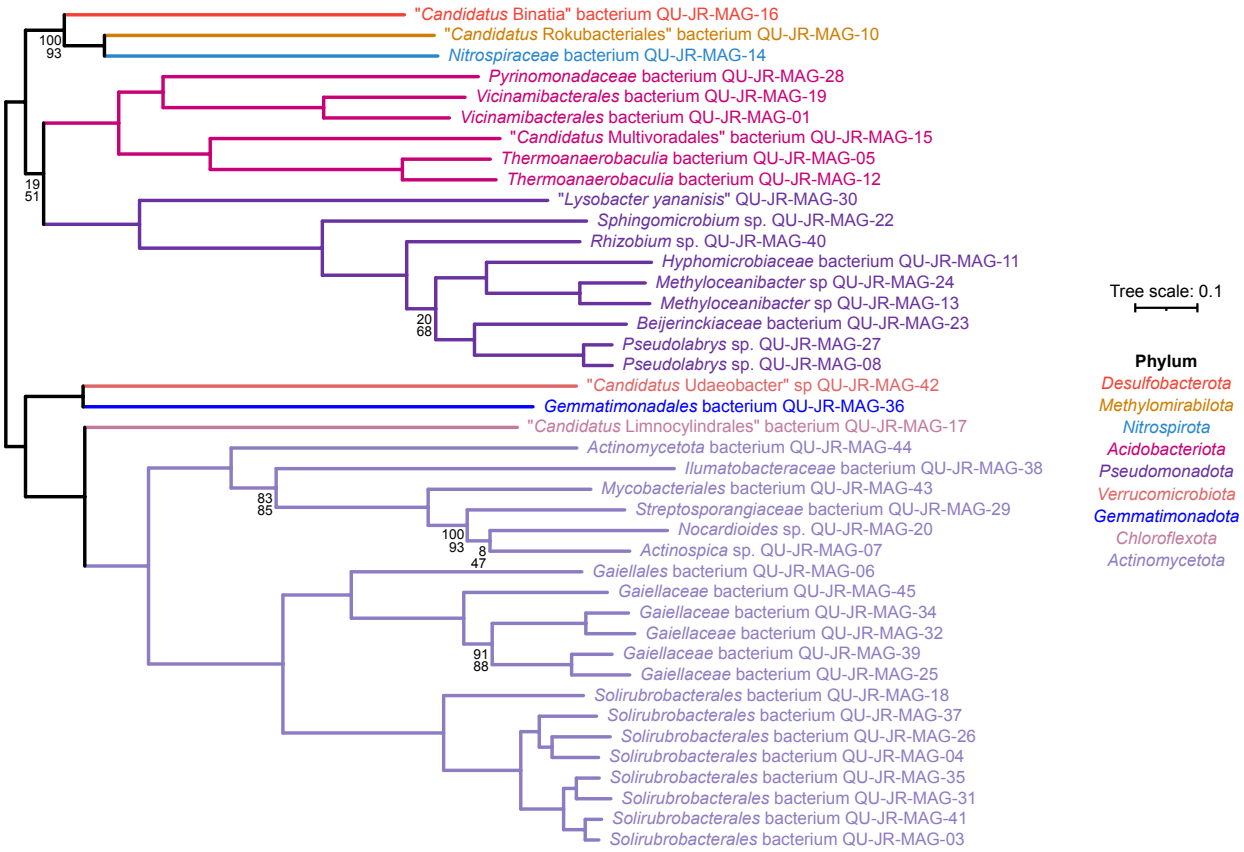

Figure 6. Unrooted phylogeny of the bacterial MAGs generated in this study. An unrooted, maximum likelihood phylogeny of the 41 high-quality metagenome-assembled genomes (MAGs) generated in this study, prepared from a concatenated alignment of the bac120 gene set of the Genome Taxonomy Database. Taxa names and branches are colour coded based on phylum. The scale represents the mean number of nucleotide substitutions per site. The numbers on the nodes indicate the SH-aLRT support values (top numbers) and the ultra-fast jackknife values using a 40% resampling rate (bottom numbers), both calculated from 1000 replicates; values are only shown at nodes where at least one value is below 95.